

UNVEILING THE BACKBONE-OPTIMIZER COUPLING BIAS IN VISUAL REPRESENTATION LEARNING

Siyuan Li^{1,2,*} Juanxi Tian^{1,*} Zedong Wang^{1,*} Luyuan Zhang¹ Zicheng Liu^{1,2}
Weiyang Jin¹ Yang Liu³ Baigui Sun³ Stan Z. Li^{1,†}

¹AI Lab, Research Center for Industries of the Future, Westlake University, Hangzhou, China

²Zhejiang University, Hangzhou, China

³Damo Academy, Hangzhou, China

ABSTRACT

This paper delves into the interplay between vision backbones and optimizers, unveiling an inter-dependent phenomenon termed *backbone-optimizer coupling bias* (BOCB). We observe that canonical CNNs, such as VGG and ResNet, exhibit a marked co-dependency with SGD families, while recent architectures like ViTs and ConvNeXt share a tight coupling with the adaptive learning rate ones. We further show that BOCB can be introduced by both optimizers and certain backbone designs and may significantly impact the pre-training and downstream fine-tuning of vision models. Through in-depth empirical analysis, we summarize takeaways on recommended optimizers and insights into robust vision backbone architectures. We hope this work can inspire the community to question long-held assumptions on backbones and optimizers, stimulate further explorations, and thereby contribute to more robust vision systems. The source code and models are publicly available.

1 INTRODUCTION

The past decade has witnessed rapid progress in computer vision, marked by significant strides in network architectures (He et al., 2016; Dosovitskiy et al., 2021; Yu et al., 2024) and optimizers (Sinha & Griscik, 1971; Kingma & Ba, 2015). From AlexNet (Krizhevsky et al., 2012a) to ConvNeXt (Liu et al., 2022a), the vision community has pushed the boundaries of pre-trained backbones in terms of task-specific accuracy, efficiency (e.g., model parameters and inference speed), and other metrics through heuristic architecture designs. Amidst the buzz, however, the impact of optimizers has been largely overlooked - practitioners often default to established ones without systematic justification. For instance, while AdamW (Loshchilov & Hutter, 2019) has emerged as the de facto choice for training Vision Transformers (ViTs), the generality of such optimizer preferences across backbones remains under-explored. This inquiry becomes particularly important as vision models nowadays are deployed in various real-world applications, where the choice of optimizer can significantly impact model generalization (Woo et al., 2023; Oquab et al., 2023), robustness to distribution shifts (Vishniakov et al., 2023), and adaptability in transfer learning (He et al., 2017; Kirillov et al., 2023). Thus, understanding the backbone-optimizer interplay may provide critical insights for enhancing model reliability and facilitating vision backbone design and deployment across diverse practical scenarios.

In this paper, we explore the relationship between vision backbones and optimizers. Our primary focus is threefold: (i) Does any identifiable dependency exist between existing vision backbones and widely-used optimizers? (ii) If such backbone-optimizer dependencies exist, (how) do they affect the training dynamics and performance of vision models? (iii) Can we identify direct connections between these inter-dependencies and specific designs of vision backbone architectures and optimizers?

To answer these questions, we first revisit different categories of existing vision backbones and optimizers as shown in Figures 1, 2, and Section 2. We then conduct extensive experiments where 20 representative backbones are evaluated against 20 optimizers on mainstream vision datasets, including CIFAR-100 (Krizhevsky et al., 2009), ImageNet (Krizhevsky et al., 2012b), and COCO (Lin et al., 2014). As such, we provide the backbone-optimizer benchmark and thereby observe an interesting inter-dependent phenomenon, which we term *backbone-optimizer coupling bias* (BOCB). Table 1 conveys this evidence: classical Convolutional Neural Networks (CNNs) like VGG (Simonyan &

*Equal contribution. †Corresponding author.

Zisserman, 2015) and ResNet (Zhang et al., 2022) exhibit a marked co-dependency with SGD (Sinha & Griscik, 1971). In contrast, modern backbones, such as Vision Transformers (ViTs) (Dosovitskiy et al., 2021) and ConvNeXt (Liu et al., 2022a), perform better when paired with adaptive learning rate optimizers (Loshchilov & Hutter, 2019) (see blue and gray results in Table 1). While most backbones and optimizers are assumed to be unbiased and well-generalized, our findings appear to question it.

To dig deep into such interplay, thorough empirical analyses are conducted from both backbone and optimizer perspectives. We first examine the performance stability of each backbone with violinplots as shown in Figure 3, which offers intuitive insights into their robustness across different optimizers. We then analyze the hyper-parameter robustness of all benchmarked backbone-optimizer pairs in Figure 4,5, as the well-designed ones are expected to have robust hyper-parameter settings. To further elucidate the rationale behind BOCB, we visualize the layer-wise patterns and PL exponent alpha metrics (Martin et al., 2021) of learned parameters to examine how different network architectures influence the parameter space and optimization complexity, hence potentially inducing the BOCB phenomenon. As illustrated in Figures 1, 6, and Appendix C, certain stage-wise (hierarchical or isotropic) and block-wise (heterogeneous or not) designs can significantly affect parameter space and hyper-parameters robustness. Interestingly, we further observe that optimizers also introduce *bias* back to backbones (see Section 4). For example, fine-tuning the AdamW pre-trained backbones with the other ones often leads to significant performance degradation, while this is not present when pre-training the model with SGD variants. Moreover, different pre-training optimizers may even alter the parameter patterns of identical backbones. Overall, our findings suggest that BOCB can be introduced by optimizers and backbones and may significantly impact both the pre-training and downstream fine-tuning of vision models, thus limiting their flexibility and practical applications.

In the following sections, we first provide an overview of vision backbones and optimizers in Section 2. We then present the backbone-optimizer benchmark details and our empirical findings in Section 3. Section 4 offers an in-depth analysis of the rationale behind BOCB and takeaways for recommended optimizers and summarized backbone designs. Our main contributions can be summarized as follows:

- We explore the crucial yet poorly studied backbone-optimizer interplay in visual representation learning, revealing the phenomenon of *backbone-optimizer coupling bias* (BOCB).
- We provide the backbone-optimizer benchmark that encompasses 20 popular vision backbones, from classical CNNs to recent transformer-based architectures, and evaluate their performance against 20 mainstream optimizers on CIFAR-100, ImageNet-1K, and COCO, unveiling the practical limitations introduced by BOCB in both pre-training and transfer learning scenarios.
- From the BOCB perspective, we summarize optimizers recommendations and insights on more robust vision backbone design. The benchmark results also serve as takeaways for user-friendly deployment. We open-source the code and models for further explorations in the community.

2 ROADMAPS OF VISION BACKBONES AND OPTIMIZERS

This section provides an overview of most existing vision backbones and optimizers. We first revisit different networks based on their stage-wise macro design (hierarchical or isotropic), building block structures (heterogeneous or not), and core operators (convolution, self-attention, *etc.*). We then dive into mainstream optimizers, emphasizing their distinctive approaches to learning rate adjustment and gradient handling. This serves two purposes: first, it offers an organized framework for understanding the current landscape; second, it facilitates our subsequent analyses, allowing us to draw connections between experimental results and specific techniques, thereby yielding clear observations and insights.

2.1 TAXONOMY OF VISION BACKBONE ARCHITECTURES

Stage-wise Macro Design. As shown in Figure 1 and Table A1, the overall framework of existing vision backbones can be categorized into two groups: **(i) Hierarchical architectures:** These models (*e.g.*, VGG (Simonyan & Zisserman, 2015), ResNet (He et al., 2016), MobileNet.V2 (Sandler et al., 2018), and EfficientNet (Tan & Le, 2019)) divide the network into multiple downsizing stages, where each stage consists of stacked building blocks with specific designs (*e.g.*, bottleneck, MetaFormer (Yu et al., 2024) or ConvNeXt (Liu et al., 2022a)) for feature extraction. **(ii) Isotropic architectures:** In contrast, backbones like Vision Transformers (ViTs) (Dosovitskiy et al., 2021) and MLP-Mixers (Tolstikhin et al., 2021) employ an isotropic building block stacking, where stand-alone token and channel mixers (*e.g.*, self-attention and MLP) are proposed to capture long-range dependencies with attention-like operators while enabling token prompting for broader applications.

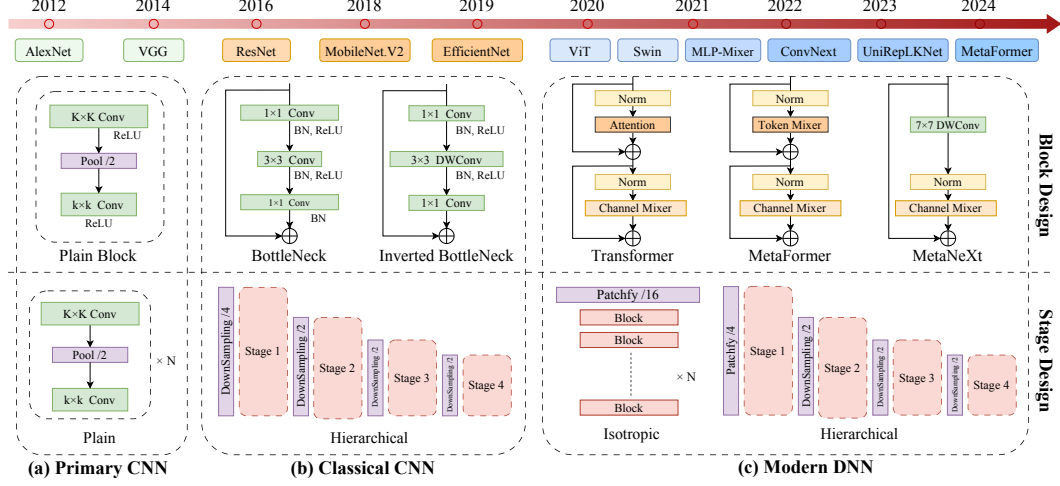


Figure 1: Vision backbones with representative macro and micro designs since 2012. **(a) Primary CNNs** like VGG laid the foundation for vision backbone design, *i.e.*, multi-layer networks built by plainly stacking building blocks. **(b) Classical CNNs** like ResNet identified the overall framework of vision backbones as hierarchical stages, each comprising stacked bottlenecks connected by overlapped downsampling layers. **(c) Modern DNNs** introduced different intra-block structures while presenting two main groups of stage-wise design: hierarchical and isotropic stages with downsampling and patchifying. We summarize all the technical details of these typical vision backbones in Table A1.

Intra-block Micro Design. The building block structures can also be classified into two paradigms: **(i) Homogeneous structures:** Early CNNs like AlexNet (Krizhevsky et al., 2012a) employed a straightforward approach of interleaving convolutions and pooling layers for feature extraction. A significant breakthrough came with the bottleneck structure of ResNet (He et al., 2016), which set a new paradigm for subsequent architectures. Following this, research has focused on enhancing bottlenecks through the integration of specialized operators, such as separable convolutions (Sandler et al., 2018) and CBAM (Woo et al., 2018). **(ii) Heterogeneous structures:** ViTs (Dosovitskiy et al., 2021; Liu et al., 2021) marked a paradigm shift by introducing heterogeneous building blocks, in which token-mixers (*e.g.*, self-attention, sliding windows) and channel-mixers (typically feed-forward networks) are exploited for disentangled feature processing. Built upon this, subsequent works mainly focus on crafting more efficient (Yu et al., 2024) and expressive (Ding et al., 2024) token-mixers. Notably, most existing studies change network architectures heuristically to improve certain metrics, such as task accuracy, speed, and parameter efficiency. However, the impact of these architectural choices on their optimization has been largely overlooked, which is exactly what we are interested in.

2.2 MAINSTREAM GRADIENT-BASED OPTIMIZERS

The optimization of DNNs is an intricate process requiring iterative parameter updates. Algorithm 1 offers a general framework for this refinement, encapsulating the essence of gradient-based optimizers. The entire pipeline includes four key steps:

Step 1: Gradient Computation. The initial phase involves calculating partial derivatives of the loss function \mathcal{L} with respect to each layer’s parameters θ_l through backpropagation. This

determines the update direction for each model parameter that can minimize the learning objectives. **Step 2: Gradient Estimation.** To further improve the optimization stability and convergence, gradients can be refined by incorporating both current and historical information. Techniques like momentum are thus employed to smooth gradient estimates, thereby providing more robust and reliable updates. **Step 3: Learning Rate Calculation.** At this stage, the critical hyper-parameter,

Algorithm 1 General Gradient-based Optimizer for DNNs

Require: DNN parameters $\theta = \{\theta_l\}_{l=1}^L$, an initial learning rate lr , weight decays $\omega = \{\omega_l\}_{l=1}^L$, a loss function \mathcal{L} , and a dataset \mathcal{D} .

- 1: Initialize parameters $\theta^0 = \{\theta_l^0\}_{l=1}^L$ and learning rates $\{\alpha_l^0\}_{l=1}^L \leftarrow \text{lr}$.
- 2: **for** each iteration $i = 1, 2, \dots, L$ **do** ▷ Loop over iterations
- 3: **for** each layer $l = 1, 2, \dots, L$ **do** ▷ Loop over layers
- 4: Compute gradients $\nabla \theta_l^{i-1} = \frac{\partial \mathcal{L}(\theta, \mathcal{D})}{\partial \theta_l}$. ▷ Step 1
- 5: Estimate the gradients g_l^i with $\nabla \theta_l^{i-1}$ and $\{g_l^j\}_{j=1}^{i-1}$. ▷ Step 2
- 6: Calculate α_l^{i-1} with $\{\alpha_l^j\}_{j=1}^{i-1}$ and $\{g_l^j\}_{j=1}^{i-1}$. ▷ Step 3
- 7: Update: $\theta_l^i \leftarrow \theta_l^{i-1} - \alpha_l^{i-1} \cdot (g_l^{i-1} + \omega_l \cdot \theta_l^{i-1})$. ▷ Step 4
- 8: **end for**
- 9: **end for**

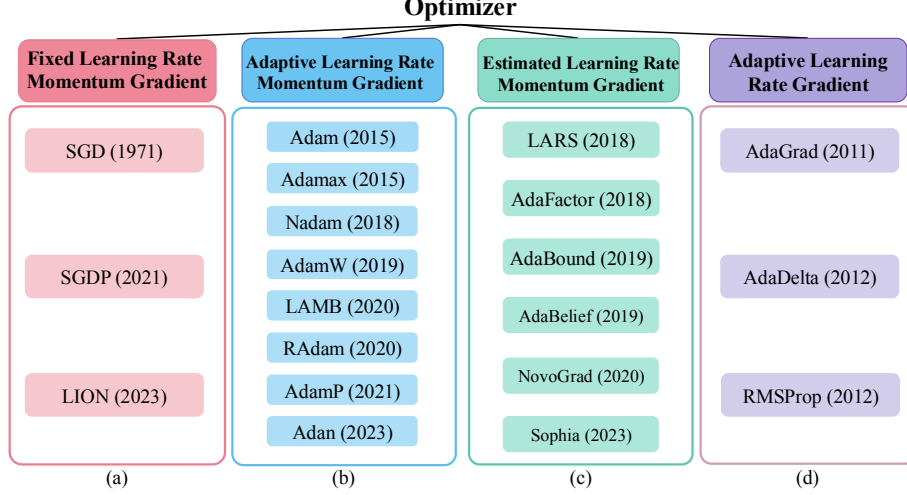


Figure 2: Overview of mainstream gradient-based optimizers, which are categorized by the techniques of learning rate adjustment (**step 2**) and gradient estimation (**step 3**) in Algorithm 1. **(a)** and **(d)** only optionally employs **step 2** (momentum gradients) or **step 3** (adaptive learning rates), while **(b)** and **(c)** consider both of them. **(b)** employs adaptive learning rates by estimating second moments; **(c)** estimates the dynamic learning rate by other gradient components except for the second moments.

learning rate, is calculated according to the past statistics and estimated gradients through adaptive optimizers (*e.g.*, AdaGrad, RMSProp, and Adam) for better convergence. **Step 4: Parameter Update.** The final step updates the network parameters θ_l with refined gradients g_l , learning rates α_l , and a weight decay term ω_l while incorporating additional regularization policies to mitigate overfitting.

As such, mainstream optimizers can be divided into four principal classes as depicted in Figure 2. **(a) Fixed Learning Rate with Momentum:** This category employs static learning rates while modulated by momentum (Sinha & Griscik, 1971; Heo et al., 2021). Its key principle is the accumulation of past gradients to determine the current update, which aids in accelerating convergence in consistent directions while dampening oscillations in high-curvature dimensions. **(d) Adaptive Learning Rate without Momentum:** Optimizers in this class (*e.g.*, AdaGrad (Duchi et al., 2011) and RMSProp (Hinton, 2012)) adapt learning rates for each parameter based on the historical statistics. While this approach may introduce extra cost, it allows for larger updates for infrequent parameters and smaller updates for frequent ones, providing better adaptability to varying feature scales and data sparsity. **(b) Adaptive Learning Rate with Momentum:** This type combines the benefits of momentum with parameter-wise learning rate adaptation (Kingma & Ba, 2015; Reddi et al., 2018), making it well-suited for large datasets or complex neural networks. **(c) Estimated Learning Rate with Momentum:** These optimizers aim to mitigate the convergence issues of **Category (b)** through additional constraints or estimations, such as factored moments (Shazeer & Stern, 2018) and bounded learning rates (Luo et al., 2019).

3 BACKBONE-OPTIMIZER COUPLING BIAS (BOCB)

3.1 COMBINED EVALUATION OF BACKBONE AND OPTIMIZER

It is commonly assumed that both backbones and optimizers should be broadly applicable and can be combined freely without significant inter-dependence. To investigate the potential backbone-optimizer interplay between a set of vision backbones $\{\mathcal{F}_i(\cdot; \theta)\}_{i=1}^{N_b}$ and widely used optimizers $\{\mathcal{O}_j(\cdot)\}_{j=1}^{N_o}$, we consider three different aspects of evaluation, from task-specific accuracy to optimization dynamics, to identify and then explain the BOCB phenomena (if it exists) with a standard benchmark.

(A) Performance Metrics. We assess each backbone-optimizer combination with the top-1 accuracy on the validation set to study whether a backbone relies on (or fails with) the certain optimizer. Given a backbone \mathcal{F}_i and a set of its results $R_i = \{r_j(\mathcal{F}_i)\}_{j=1}^{N_o}$, we detect the failure case that is dynamically lower than others with quantiles and a threshold $\gamma > 0$,

$$r_j(\mathcal{F}_i) < \max(R_i) - \min(Q_{0.75}(R_i) - Q_{0.25}(R_i), \gamma). \quad (1)$$

Meanwhile, the severity of BOCB can also be reflected by the standard deviation (Std) and range. Therefore, we report these statistics by removing the worst result $\min(R_i)$, and highlight the top-4

results in blue while marking the failed attempts in gray, which yields a heatmap-like table of benchmarking results as a clear overview of the effectiveness of each backbone-optimizer combination.

(B) Hyper-parameter Robustness. While standard metrics offer basic insights, we delve deeper into the adaptability of these backbone-optimizer pairs through the lens of hyper-parameter robustness. To quantify this stability, we measure the *variation* of all optimal optimizer hyper-parameters from their mode (most common) configurations. Assuming there are n optimal learning rates and m optimal weight decays for all backbone-optimizer pairs, we convert these values into discrete one-hot codes $\{\tilde{r}_i\}_{i=1}^n$ and $\{\tilde{\omega}_i\}_{i=1}^m$, calculate mode statistics M_{lr} and M_{ω} , and measure the *variation* by Manhattan distance $\sum_{i=1}^n |\tilde{r}_i - M_{lr}| + \sum_{i=1}^m |\tilde{\omega}_i - M_{\omega}|$. Lower variation often denotes greater robustness of hyper-parameter settings and thereby indicates desirable adaptability to new or poorly studied optimizers or vision backbones and thus could be desirable for broader practical applications.

(C) Parameter Patterns and Convergence Quality. To gain intuitive insights into different network architectures, we analyze the learned parameters with four key indicators, including PL exponent alpha (Martin et al., 2021), entropy, L_2 -norm, and top- k PCA energy ratio. Please view Appendix A.3 for our detailed interpretations. This analysis reveals intrinsic topological patterns that reflect the typical layer-wise properties of various backbones, as shown in Figure 6 and Appendix C. We observe distinct entropy patterns in hierarchical versus isotropic macro designs, variations in L_2 -norm across stages, and changes in PCA energy ratios for diverse layer types (e.g., convolutional vs. attention-based). By analyzing these patterns, we gain valuable insights into how different network architectures interact with various optimization algorithms, furthering our understanding of the BOCB phenomenon and informing future design choices for both backbones and optimizers.

3.2 BENCHMARKS AND OBSERVATIONS

Benchmark Settings. We conduct the main benchmark of vision backbones and optimizers for image classification on CIFAR-100 (Krizhevsky et al., 2009) for analysis efficiency, where models are trained 200 epochs with optimal hyper-parameters for various optimizers. We select 20 representative vision backbones from the **three** categories with similar parameters counts, as summarized in Table A1: **(a)** Primary CNNs include AlexNet (Alex) (Krizhevsky et al., 2012a) and VGG-13-BN (VGG) (Simonyan & Zisserman, 2015); **(b)** Classical CNNs include ResNet-50 (R) (He et al., 2016), DenseNet-121 (DN) (Huang et al., 2017), MobileNet.V2 (MobV2) (Sandler et al., 2018), EfficientNet-B0 (Eff) (Tan & Le, 2019), and RepVGG (Ding et al., 2021); **(c)** Modern DNNs include Transformers (DeiT-S (Touvron et al., 2021a) and Swin-T (Liu et al., 2021)), MLP-Mixer-S (MLP) (Tolstikhin et al., 2021), modern CNNs include ConvNeXt-T (CNX) (Liu et al., 2022a), ConvNeXt.V2 (CNXV2) (Woo et al., 2023), MogaNet-S (Moga) (Li et al., 2024), and UniRepLKNNet-T (URLK) (Ding et al., 2024). We also evaluate MetaFormer baselines (Yu et al., 2024) with IdentityFormer-S12 (IF), PoolFormerV2-S12 (PFV2), ConvFormer-S12 (CF), and AttentionFormer-S12 (AF), whose only difference is their token-mixer designs. We also selected 20 popular optimizers from the **four** categories as discussed in Figure 2: **(a) Fixed Learning Rate with Momentum** includes SGD-M (Sinha & Griscik, 1971), SGDP (Heo et al., 2021), and LION (Chen et al., 2023); **(b) Adaptive Learning Rate with Momentum** covers Adam (Kingma & Ba, 2015), AdaMax (Kingma & Ba, 2015), AdamP (Heo et al., 2021), AdamW (Loshchilov & Hutter, 2019), LAMB (You et al., 2020), NAdam (Reddi et al., 2018), RAdam (Liu et al., 2020), and Adan (Xie et al., 2023). **(c) Estimated Learning Rate with Momentum** involves AdaBelief (Zhuang et al., 2020), AdaBound (Luo et al., 2019), AdaFactor (Shazeer & Stern, 2018), LARS (Ginsburg et al., 2018), NovoGrad (Ginsburg et al., 2020), and Sophia (Liu et al., 2023); **(d) Adaptive Learning Rate without Momentum** comprises AdaGrad (Duchi et al., 2011), AdaDelta (Zeiler, 2012), and RMSProp (Hinton, 2012). We consider two training recipes: (1) PyTorch-style training (Szegedy et al., 2016) with basic augmentations, (2) DeiT-style training (Touvron et al., 2021a) with advanced augmentations (Cubuk et al., 2020; Zhang et al., 2018) and techniques (Huang et al., 2016). As for **optimizer hyper-parameters**, we first search the two commonly-employed ones (learning rate and weight decay) with NNI toolbox (Microsoft, 2021), i.e., determining the NNI search range manually. Subsequently, we tune other optimizer-specific hyper-parameters (e.g., momentum in SGD and β_2 in Adam). The average top-1 accuracy over three trials is reported. Please refer to Appendix A.1 for further implementation specifics.

Observations. As shown in Table 1, we observed an interesting phenomenon that some popular models (e.g., DeiT-S and ConvNeXt-T) yield bad results with some optimizers (i.e., SGD and LARS). Therefore, we summarize this phenomenon as BOCB, where the performance of a certain visual architecture is strongly coupled with the choice of the optimizer, deviating from the expected independence between network designs and optimization algorithms. In particular, we notice that classical

Table 1: Top-1 accuracy (%) of representative vision backbones with 20 popular optimizers on CIFAR-100. The torch-style training settings are used for AlexNet, VGG-13, R-50 (ResNet-50), DN-121 (DenseNet-121), MobV2 (MobileNet.V2), and RVGG-A1 (RepVGG-A1), while other backbones adopt modern recipes, including Eff-B0 (EfficientNet-B0), ViT variants, ConvNeXt variants (CNX-T and CNXV2-T), Moga-S (MogaNet-S), URLK-T (UniRepLKNNet-T), and TNX-T (TransNeXt-T). We list MetaFormer S12 variants apart from other modern DNNs as IF-12, PFV2-12, CF-12, AF-12, and CAF-12. Two bottom lines report mean, std, and range on statistics that removed the worst result for all models.

Optimizer	AlexNet	VGG-13	R-50	DN-121	MobV2	Eff-B0	RVGG-A1	DeiT-S	MLP-S	Swin-T	CNX-T	CNXV2-T	Moga-S	URLK-T	TNX-T	IF-12	PFV2-12	CF-12	AF-12	CAF-12
SGD-M	66.76	77.08	78.76	78.01	77.16	79.41	75.85	63.20	72.64	78.95	60.09	82.25	75.93	82.75	86.21	77.40	77.70	83.46	83.02	81.21
SGDP	66.54	77.56	79.25	78.93	77.32	79.55	75.26	63.53	69.24	80.56	61.25	82.43	80.86	82.18	86.12	77.55	77.53	83.54	82.88	81.56
LION	62.11	73.87	75.28	75.42	74.62	76.97	73.55	74.57	74.19	81.84	82.29	82.53	85.03	83.43	86.96	78.65	79.66	84.62	82.41	79.59
Adam	65.29	73.41	74.55	76.78	74.56	76.48	75.06	71.04	72.84	80.71	82.03	82.66	84.92	84.73	86.23	78.39	79.18	84.81	81.54	82.18
Adamax	67.30	73.80	75.21	73.52	74.60	78.37	74.33	73.31	73.07	81.28	80.25	81.90	84.51	83.81	86.34	78.02	79.55	84.31	81.83	82.50
NAdam	60.49	73.96	74.82	76.10	75.08	77.06	74.86	72.75	73.77	81.80	82.26	82.72	85.23	82.07	86.44	78.37	80.32	84.81	81.82	82.83
AdamW	62.71	73.90	75.56	78.14	76.88	78.77	75.35	72.15	73.59	81.30	83.52	83.59	86.19	86.30	87.51	79.39	80.55	85.46	82.24	83.60
LAMB	66.90	75.55	77.19	78.81	77.59	78.77	77.04	75.39	74.98	83.47	84.13	84.93	86.04	84.99	87.37	80.21	80.01	85.40	83.16	83.74
RAdam	61.69	74.64	75.19	76.40	75.94	77.08	74.83	72.41	72.11	79.84	82.18	82.69	84.95	84.26	86.49	78.46	79.71	84.93	81.44	82.35
AdamP	60.27	75.56	78.17	78.89	77.79	78.65	77.67	71.55	73.66	80.91	84.47	84.40	86.45	86.19	87.16	79.20	81.70	85.15	82.12	83.40
Adan	63.98	74.90	77.08	79.33	77.73	78.43	76.99	76.33	74.94	83.35	84.65	84.77	86.46	86.75	87.47	80.59	83.23	85.58	83.51	84.89
AdaBound	66.59	77.00	78.11	75.26	78.76	79.88	74.14	68.59	70.31	80.67	71.96	83.90	78.48	83.03	86.07	77.99	77.81	82.73	83.08	82.38
LARS	64.35	75.71	78.25	77.25	76.23	72.43	75.50	71.36	72.64	81.29	61.40	82.22	33.26	41.03	85.16	77.66	78.78	82.98	81.00	82.05
AdaFactor	63.91	74.49	75.41	77.03	75.38	77.83	75.03	74.02	71.16	80.36	82.82	83.06	85.17	85.99	86.57	78.78	78.81	84.90	81.94	82.36
AdaBelief	62.98	75.09	80.53	79.26	75.78	78.48	76.90	70.66	73.30	80.98	83.31	84.47	84.80	84.54	86.64	78.55	81.01	85.03	83.21	83.56
NovoGrad	64.24	76.09	79.36	77.25	71.26	74.23	75.16	73.13	67.03	81.82	79.99	82.01	82.96	80.77	85.85	77.16	78.92	83.51	81.28	82.98
Sophia	64.30	74.18	75.19	77.91	76.60	78.95	75.85	71.47	72.74	80.61	83.76	83.94	85.39	84.20	86.60	77.67	78.90	84.58	81.67	82.96
AdaGrad	45.79	71.29	73.30	51.70	33.87	77.93	46.06	67.24	67.50	75.83	75.63	50.34	83.03	82.57	66.83	44.34	44.40	79.67	78.71	38.09
AdaDelta	66.87	74.14	75.07	76.82	75.32	77.88	74.58	65.44	71.32	80.25	74.25	82.74	81.06	84.17	85.31	75.91	76.40	84.05	82.62	82.08
RMSProp	59.33	73.30	74.25	75.45	73.94	76.83	74.92	70.71	71.63	77.52	82.29	82.11	85.17	61.14	86.21	77.40	77.14	84.01	79.72	81.83
Mean	63.67	74.68	76.31	76.94	75.65	77.77	75.19	70.82	72.10	80.63	78.13	82.92	83.51	82.40	86.34	78.03	78.94	84.28	81.99	82.32
Std/Range	1.1/8	1.0/4	1.6/6	1.4/6	1.6/8	1.2/6	0.9/4	2.9/13	1.7/8	1.1/6	8.0/25	0.8/3	2.8/11	5.5/26	0.6/2	0.8/5	1.2/7	0.8/3	0.9/4	0.9/5

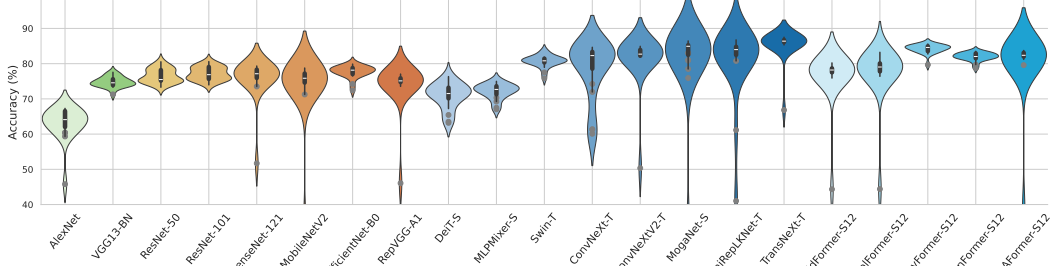


Figure 3: **Violinplot of the performance stability for different backbones.** We visualize the results in Table 1 as violinplots to show the performance stability of different vision backbones. In particular, favorable backbones should not only achieve great performance (high mean accuracy) with few optimizers but yield a small performance variance (a flat distribution without outliers). Note that grey dots denote the outliers (backbone-optimizer combination with poor results), revealing the phenomenon of BOCB. We suggest that well-designed (vision) backbones should exhibit both superior performance and great performance stability across optimizers to mitigate the risk of BOCB.

CNNs (*e.g.*, VGG, ResNets, and RepVGG) exhibit a slight coupling with **Category (a)** optimizers but have not encountered evident BOCB. In contrast, modern architectures like ViTs (Dosovitskiy et al., 2021) and ConvNeXt (Liu et al., 2022a) strongly matched with adaptive optimizers in **Category (b)**.

As observed in Figure 3, we assume that such a coupling bias may stem from the increasing complexity of optimization as network architectures evolve. Concretely, modern backbones incorporate complex designs such as advanced token-mixers (*e.g.*, MogaNet and UniRepLKNNet) and block-wise heterogeneous structures (*e.g.*, ConvNeXt variants and CAFormer), which shape a more intricate and challenging optimization landscape, necessitating adaptive learning rate strategies. Thus, modern backbones exhibit stronger couplings with optimizers that can navigate these complex landscapes. As we meet real-world challenges, it becomes critical to explore network architectures beyond traditional metrics. Optimizers provide an entry point for this investigation. Intuitively, different network architectures might seemingly affect the optimization landscape, thereby influencing the optimization process. We assume that this interplay between backbones and optimizers may have substantial implications for both pre-training and fine-tuning in practical applications. By examining this relationship, we aim to provide insights that can guide the development of more effective and

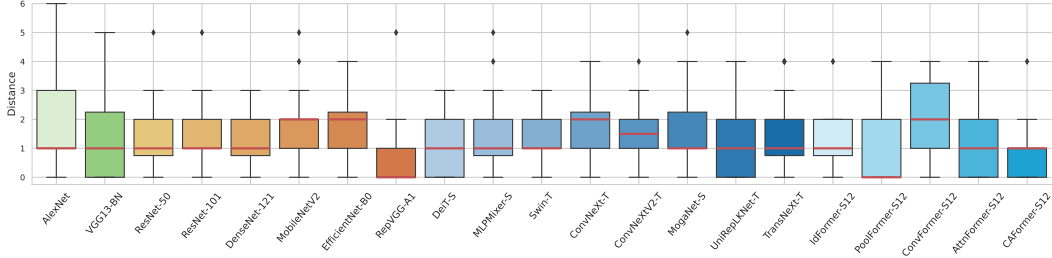


Figure 4: **Boxplot visualization of hyper-parameter robustness** (learning rate and weight decay) for various backbones on CIFAR-100. The vertical axis denotes variation (measured by Manhattan distances) of all optimal hyper-parameters for certain backbones across different optimizers to the default (mode) values. Holistically, backbones with larger mean and variance of variations (*e.g.*, AlexNet, EfficientNet-B0, ConvNeXt-T, and ConvFormer-S12) require more tuning efforts in practice and may be tough to adapt to new or poorly-studied optimizers and tasks. In contrast, models with low variation maximum while the small medians (*e.g.*, ResNet-50, RepVGG-A1, and CAFormer-S12) are regarded as more robust and with more favorable optimization behavior from the view of optimizers.

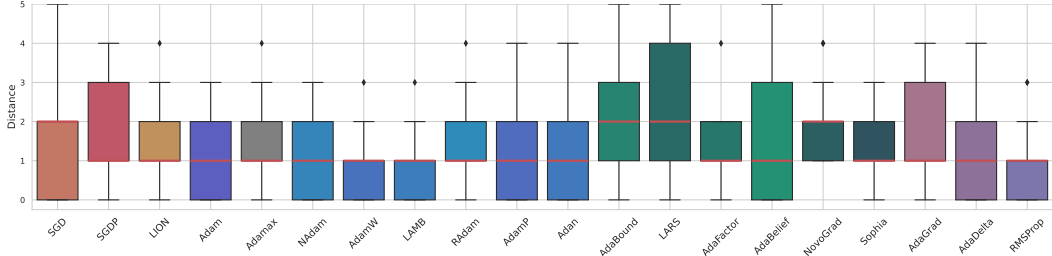


Figure 5: **Boxplot of optimizers generality** across different backbones on CIFAR-100. Symmetrical to Figure 4, the analysis scope here is switched from backbones to optimizers so as to showcase the optimizer’s generality from the perspectives of hyper-parameter robustness. Some optimizers in **Category (b)** show favorable robustness (*e.g.*, AdamW and LAMB). Contrastively, several optimizers in the other three types show poor generality (*e.g.*, SGDP, AdaBound, and LARS), which are excluded from our further discussion on the connection between BOCB and diverse vision backbone designs.

efficient models for computer vision tasks. The BOCB phenomenon has also several implications for vision backbones in terms of user-friendly deployment and more robust architecture design:

(A) Deployment. Vision backbones with weaker BOCB offer greater flexibility and are more user-friendly, especially for practitioners with limited resources for extensive hyper-parameter tuning. However, modern architectures like ViTs and ConvNeXt, which exhibit strong coupling with adaptive optimizers, require careful optimizer selection and hyper-parameter tuning for optimal performance.

(B) Performance and Generalization: While weaker coupling offers more user-friendliness, stronger coupling can potentially lead to better performance and generalization. Tailoring the optimization process to certain architectural characteristics of modern backbones, such as stage-wise hierarchical structures and attention mechanisms for token mixing, can more effectively navigate complex optimization landscapes, unlocking superior performance and generalization capabilities.

(C) Backbone Design Insights: The observed BOCB phenomenon highlights the need to consider the coupling between backbone designs and optimizer choices. When designing new backbone architectures, it is crucial to account for both the inductive bias (*e.g.*, hierarchical structures and local operations) and some optimizing auxiliary modules (Touvron et al., 2021b; Shleifer et al., 2021) introduced by the macro design principles. A balanced approach that harmonizes the backbone design with the appropriate optimizer choice can lead to optimal performance and efficient optimization, enabling the full potential of the proposed architecture to be realized.

4 WHERE DOES BOCB COME FROM?

To investigate the essence behind the BOCB phenomenon, we first consider what matters the most: optimizers or backbones. As shown in Figure 5 and Table 1, four groups of optimizers show different extents of BOCB with vision backbones. Categories (b) and (c) exhibit a robust, hyperparameter-insensitive performance peak, adept at navigating the complex optimization landscapes of early-stage

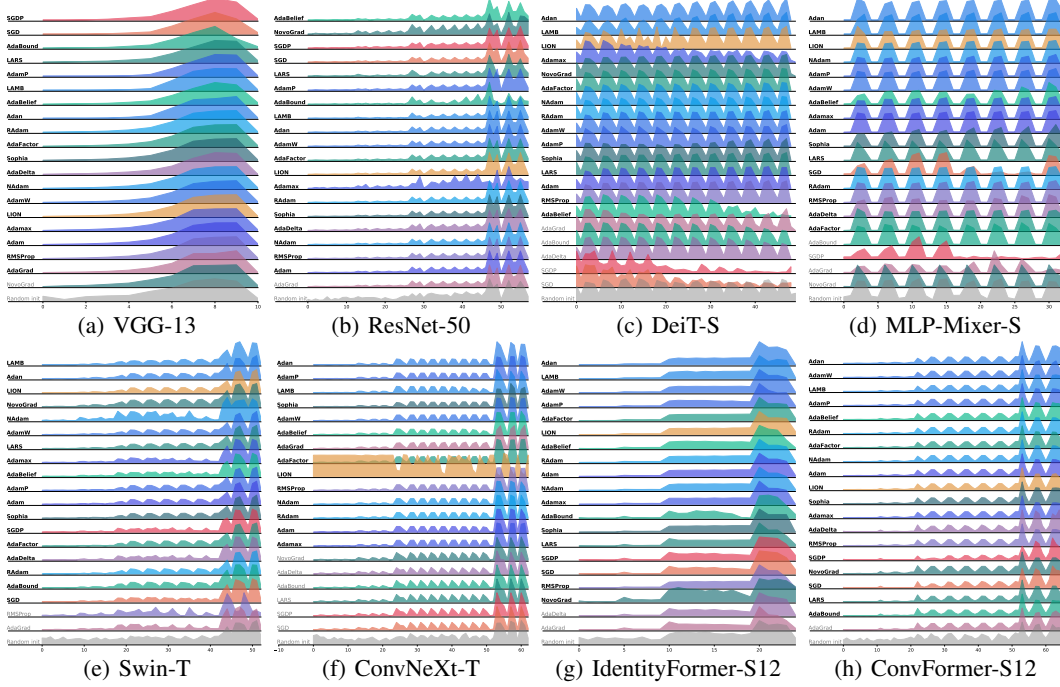


Figure 6: **Layer-wise backbone parameter patterns.** We visualize the ridge plot of the entropy patterns of learned parameters of specific vision backbones on CIFAR-100. For the sub-figure of each optimizer, the X and Y axes indicate the layer indexes and the entropy of weights, respectively.

CNNs and recent backbones. **Category (a)** necessitates meticulous hyper-parameter tuning for classical CNNs while demonstrating less adaptability to the high optimization demands of modern backbones with complex designs. **Category (d)** shows the worst performances with heavy BOCB.

4.1 ORIGINS OF BOCB: BACKBONE MACRO DESIGN AND TOKEN MIXERS

As discussed in Figure 1 and Section 2, the trajectory of vision backbones has significantly sculpted the optimization landscape, progressing through distinct phases that reflect the intricate relationship between network complexity and training challenges (as illustrated in). This section delves into the evolution of vision backbone macro design and its profound implications for the BOCB phenomenon.

(i) Early-stage CNNs: These architectures featured a straightforward design of plainly stacked convolutional and pooling layers, culminated by fully connected layers. Such a paradigm was effective but set the stage for further optimization of landscape alterations. **(ii) Classical CNNs:** The introduction of ResNet extracted a pivotal shift towards stage-wise hierarchical designs, significantly enhancing feature extraction and representation learning ability. ResNet-50, in particular, demonstrated a well-balanced approach to BOCB, which exhibited strong compatibility with SGD optimizers and a relatively lower BOCB compared to its contemporaries. **(iii) Modern Architectures:** The transition to modern backbones introduced simplified block-wise designs (e.g., MetaNeXt (Yu et al., 2023) and ConvNeXt variants (Liu et al., 2022a; Woo et al., 2023), or complex block-wise heterogeneous structures (e.g., MogaNet (Li et al., 2024) and UniRepLKNet (Ding et al., 2024)), increasing the optimization challenge and the degree of BOCB due to their complex feature extraction. Representing a pinnacle in evolution, the MetaFormer architecture incorporates both stage-wise and block-wise heterogeneity into its design. This innovative macro design refines the optimization landscape by harmonizing with optimizers, leading to reduced BOCB and enhanced performance.

The above backbone evolution underscores the pivotal role of macro design in shaping the optimization landscape and the necessity for continued innovation in backbone architectures. It highlights the delicate balance that must be struck between advancing representational capabilities and maintaining optimization efficiency. Please view Appendix C for implementation details.

Next, we illustrate three cases that elucidate how the overall framework and token mixer designs impact the BOCB phenomena with the parameter quality metric α (Martin et al., 2021), demonstrating the representational capacity versus the BOCB effect trade-off.

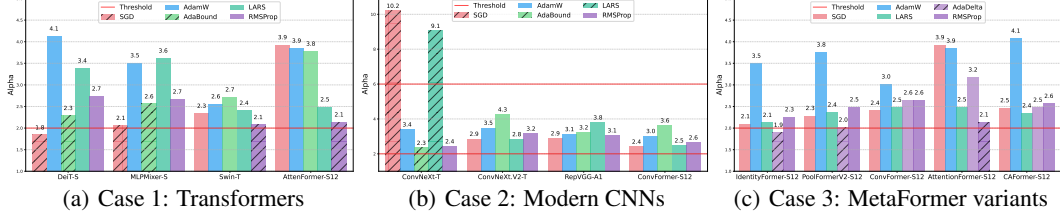


Figure 7: **BOCB case studies with PL exponent alpha metrics** (Martin et al., 2021) of learned model parameters with diverse optimizers on CIFAR-100. The alpha metric measures the fitting quality of models to a certain task, and a smaller alpha value indicates better fitting. Empirically, values less than 2 or greater than 6 have the risk of overfitting or underfitting. The diagonal bars denote the BOCB occurring. View discussions in Section 4 and details on the alpha metric in Appendix A.3.

Case 1: Transformers. The lack of inductive biases in ViTs, such as local connectivity and shift-invariance in CNNs, stems from their self-attention mechanism and stage-wise isotropic design. As shown in Figure 7(a), this necessitates careful refinements to ensure effective generalization and reduce BOCB in vision tasks. MLP-Mixer streamlines the model by replacing attention-based token mixers with MLPs, simplifying token interactions and thus inducing a more stable training process. However, it sacrifices the model’s capacity to capture long-range dependencies, which is also essential for specific vision tasks, thus representing a trade-off between model simplicity and representation capacity. AttenFormer effectively mitigates BOCB due to its MetaFormer framework, which incorporates balanced designs and residual scaling across stages. Swin-T, akin to DeiT-S, is based on vanilla Transformer but introduces hierarchical stages and local attention blocks. These designs enhance the model’s ability to capture fine-grained features, leading to better performance and weaker BOCB compared to DeiT-S. **Takeaway:** *Block-wise macro designs aimed at reducing heterogeneity or enhancing homogeneity, combined with hierarchical stages and the integration of inductive biases within token mixers, are crucial for ViTs to mitigate BOCB in computer vision tasks.*

Case 2: Modern CNNs. ConvNeXt, inspired by the success of ViTs, introduces a homogeneous block design that integrates two types of mixers within a residual connection, potentially enhancing optimization across various tasks and data scales. The effectiveness of this architecture underscores the need to evaluate network designs beyond common metrics, especially in the context of optimization and real-world challenges. The interaction between network backbones and optimizers is crucial for both pre-training and fine-tuning, with different architectures influencing the optimization landscape. BOCB in CNNs is often associated with the FFN designs, which are pivotal in models like ConvNeXt. These blocks, implemented as point-wise convolutions or inverted bottleneck layers, are susceptible to overfitting without proper regularization. ConvNeXt.V2 introduces Global Response Normalization (GRN) into FFN blocks, similar to RMSNorm, to stabilize training and prevent model collapse, thereby reducing BOCB. ConvFormer, based on the MetaFormer framework, uses homogeneous blocks with Depthwise and Pointwise Convolutions, improving training robustness and reducing BOCB risk. Similarly, the VGG series, with its simple and homogeneous architecture, exhibits well-behaved training dynamics, and RepVGG’s introduction of training-phase residual connections enhances performance while maintaining stability and avoiding BOCB (see Figure 7(b)). In contrast, ConvNeXt.V1 and MogaNet, featuring complex operations and heterogeneous blocks, are more susceptible to BOCB. UniRepLKNNet, however, sidesteps this issue with a more homogeneous design, highlighting the importance of architectural uniformity in reducing BOCB. **Takeaway:** *For modern CNNs, designs that foster a homogeneous building block structure and incorporate crafted strategies to mitigate model failures are more likely to achieve stable FFN training and reduce the risk of BOCB.*

Case 3: MetaFormer. MetaFormer architecture is distinguished by its hierarchical stage-wise and block-wise design, featuring ResScale, which facilitates the flexible integration of various token mixers. This macro design is crucial for achieving competitive performance while minimizing the risk of BOCB. IdentityFormer, with its basic identity mixer, sets a robust baseline for MetaFormer but may fall short in complex tasks requiring advanced mixer representations, potentially increasing BOCB risk, as shown in Figure 7(c). PoolFormerV2 (pooling as token mixers) outperforms IdentityFormer but may overlook critical details due to the absence of self-attention nuances, leading to higher BOCB susceptibility. To enhance MetaFormer and mitigate these risks, selecting an appropriate token mixer is essential. ConvFormer integrates CNN layers into the transformer framework, balancing local inductive bias with global receptiveness to prevent attention collapse in data-limited scenarios, ensur-

Table 2: Top-1 accuracy of DeiT-S and R-50 pose estimation (Pose.) with TopDown on COCO, evaluated by mAP (%) training 300 epochs by and AP⁵⁰ (%). We employ pre-trained VGG, ResNet-50 (R-50), Swin-T, popular optimizers with and ConvNeXt-T (CNX-T) as backbones with different pre-training settings, DeiT and RSB A2 set-including 100-epoch (SGD, LARS, or RSB A3), 300-epoch (RSB A2 and tings on ImageNet-1K. Adan), and 600-epoch pre-training (RSB A1).

Backbone	DeiT-S (DeiT)	R-50 (A2)	Pre-training	2D Pose Estimation			Object Detection									
				VGG (SGD)	R-50 (SGD)	Swin-T (AdamW)	R-50 (SGD)	R-50 (LARS)	R-50 (A3)	R-50 (A2)	R-50 (A1)	R-50 (Adan)	Swin-T (AdamW)	CNX-T (AdamW)		
SGD-M	75.35	78.82	SGD-M	47.5	71.6	38.4	36.6	27.5	28.7	23.7	34.6	27.5	37.2	38.5		
SGDP	76.34	78.02	SGDP	47.3	41.2	38.9	36.6	17.6	18.5	26.8	26.7	27.4	37.2	22.5		
LION	78.78	78.92	LION	69.5	71.5	71.3	32.1	35.8	35.4	37.6	34.6	38.8	41.9	42.8		
Adam	78.44	78.16	Adam	69.8	71.6	72.7	36.2	36.2	35.8	38.3	38.4	38.6	41.9	43.1		
Adamax	77.71	78.05	Adamax	69.0	71.2	72.4	36.8	36.8	36.4	38.3	38.4	38.3	41.5	42.0		
NAdam	78.26	78.97	NAdam	69.7	71.8	71.9	36.0	36.6	36.1	38.2	38.4	38.7	41.9	43.4		
AdamW	80.38	79.88	AdamW	70.0	72.0	72.8	37.1	37.1	36.7	38.4	39.5	36.8	41.8	43.4		
LAMB	80.23	79.84	LAMB	68.5	71.5	71.7	36.7	37.5	37.7	38.6	38.9	38.6	41.8	42.6		
RAdam	78.54	78.75	RAdam	69.8	71.8	72.6	36.6	36.5	36.0	38.2	38.4	38.6	41.6	43.3		
AdamP	79.26	79.28	AdamP	69.7	71.5	72.8	36.5	37.2	36.5	38.5	38.9	38.8	41.7	43.3		
Adan	80.81	79.91	Adan	69.7	72.1	72.8	37.7	37.0	36.0	38.6	39.0	39.4	42.0	43.2		
AdaBound	72.96	75.37	AdaBound	34.0	44.9	28.4	35.9	34.2	31.9	37.0	35.0	36.7	38.8	41.2		
LARS	73.18	79.66	LARS	54.4	63.4	47.6	35.8	28.9	28.8	34.7	36.9	37.3	34.6	40.5		
AdaFactor	79.98	79.36	AdaFactor	72.8	71.7	72.7	35.6	37.0	36.4	38.5	37.8	38.7	40.5	43.1		
AdaBelief	75.32	78.25	AdaBelief	69.6	67.0	61.8	36.2	34.4	33.1	36.4	38.2	38.5	40.0	41.4		
NovoGrad	71.26	76.83	NovoGrad	64.2	70.7	69.8	35.6	27.2	26.3	35.2	28.6	38.5	40.4	39.0		
Sophia	79.65	79.13	Sophia	69.7	71.6	72.3	36.4	35.8	35.3	38.0	38.7	37.0	40.4	42.5		
AdaGrad	54.96	74.92	AdaGrad	66.0	61.2	48.4	26.4	21.9	28.3	32.7	27.1	33.7	32.9	23.7		
AdaDelta	74.14	77.40	AdaDelta	44.3	49.3	52.0	34.9	32.7	32.7	35.9	33.9	36.6	40.0	41.5		
RMSProp	78.03	78.04	RMSProp	68.8	71.6	72.5	35.3	36.2	35.6	37.8	38.3	38.7	41.5	43.1		

Table 4: Rankings of optimizers with various aspects for practical usage. Benchmarked results rank the properties of performance and hyper-parameter robustness, the BOCB property is marked as 1 or 0, and the computational overhead is ranked by the average training hours. As described in Appendix C.5, the overall ranking is estimated as the task-home message for selecting optimizers.

	SGD	SGDP	LION	Adam	Adamax	NAdam	AdamW	LAMB	RAdam	AdamP	Adan	AdaBound	LARS	AdaFactor	AdaBelief	NovoGrad	Sophia	AdaGrad	AdaDelta	RMSProp
Performance	17	15	11	9	12	8	5	2	10	3	1	14	19	6	4	13	7	20	16	18
Hyper-parameter	10	6	3	2	7	4	1	1	8	5	9	15	14	6	6	13	7	11	12	1
BOCB	1	1	1	0	1	1	0	0	0	1	0	1	1	0	1	1	0	1	1	1
Computations	1	2	2	5	5	4	5	5	5	5	6	5	2	2	5	2	5	2	5	2
Overall	16	13	10	7	12	8	2	1	11	4	3	17	20	6	5	15	9	19	18	14

ing better convergence and reducing BOCB. AttenFormer and CAFormer further explore attention mechanisms, aiming to enhance the representation capacity of MetaFormer through improved token interactions. **Takeaway:** Overall, MetaFormer architecture’s success hinges on a judicious balance between its hierarchical design and the selection of token mixers, ensuring robust performance across diverse tasks while mitigating the risk of BOCB.

4.2 PRE-TRAINING AND TRANSFER LEARNING WITH DIFFERENT OPTIMIZERS

Extending to ImageNet-1K classification. ImageNet-1K (Krizhevsky et al., 2012b) is a fundamental benchmark that gauges the classification prowess of vision models, and we further investigate whether our observations still hold on ImageNet-1K. Please view Appendix A.1 for implementation details. As shown in Table 2, DeiT-S shows stronger BOCB than ResNet-50, while optimizers of Category (b) in Figure 2 (e.g., AdamW) have shown a reliable performance peak across diverse backbones during pre-training. Their consistent efficacy is well-aligned with the extensive feature learning required by the ImageNet-1K, making them optimal choices for the initial model training phase. The efficacy of these optimizers in the pre-training phase cascades to the transfer learning process. When models transition from ImageNet-1K pre-training to tasks such as object detection with RetinaNet or pose estimation on COCO, the choice of optimizer is pivotal.

Transfer Learning on COCO. As for the analysis of transfer learning with ImageNet-1K pre-trained models, we have identified two critical findings regarding the performance of COCO tasks post-transfer. Table 3 and Figure 8 provide a clear evidence on how various backbones and optimizers

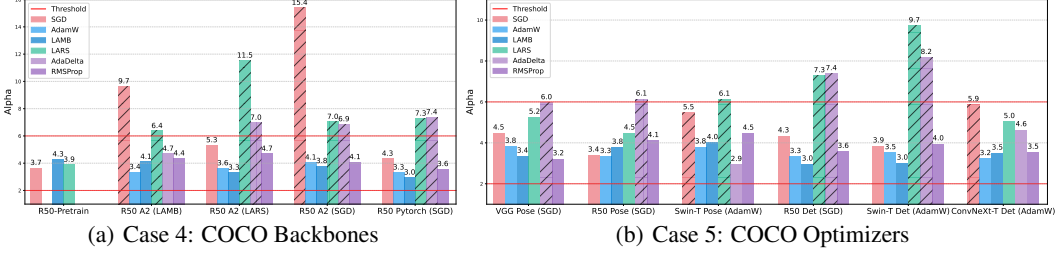


Figure 8: **BOCB case studies: PL exponent alpha metrics of different backbones and pre-training optimizers on COCO.** The alpha metric (Martin et al., 2021) measures the fitting quality of models to a certain task, and a smaller alpha value indicates better fitting. These diagonal bars denote the BOCB occurring. Please refer to the details on the alpha metric in Appendix A.3.

perform following transfer from pre-trained models to COCO detection (Lin et al., 2017). Firstly, from the backbone aspects, the backbone with a pronounced BOCB (ConvNeXt-T) continues to exhibit BOCB characteristics in transfer learning scenarios. This suggests that the inherent structural attributes of such models may not be easily mitigated through transfer learning alone. Secondly, when we controlled for the BOCB effect in the backbone by using ResNet-50, which is less susceptible to BOCB, we observed that optimizers of Category (b) and (c) may introduce significant BOCB effects during the pre-training stage despite their efficacy in pre-training, indicating that the choice of pre-training optimizer could profoundly influence the generalization and transferring abilities, thereby affecting its transferability and performance on new tasks. Moreover, unlike first-order optimizers, which do not restrict the fine-tuning phase to a specific optimizer, the optimizers in Category (b) and (c) necessitate their use in both pre-training and fine-tuning stages. **Takeaway: Optimizer selection in pre-training can significantly impact models’ transferability, with Categories (b) and (c) optimizers potentially introducing BOCB to pre-trained backbones though they exhibit superior performance. We have discussed this and summarized the practically recommended optimizers above.**

5 CONCLUSION

This paper explores the interplay of backbone designs and optimizer selections in computer vision. We unveil the phenomenon of *backbone-optimizer coupling bias* (BOCB) and the potential limitations it poses to vision backbones, for example, the extra fine-tuning time and efforts in downstream tasks. We also discover the underlying rationale behind different network designs and BOCB and thereby provide guidelines for future vision backbone design. Meanwhile, the benchmarking results and released code serve as takeaways for user-friendly deployment and evaluation. Overall, we aim to inspire the computer vision community to rethink the relationship between backbones and optimizers, consider BOCB in future studies, and thus contribute to more systematic future advancements.

Limitations. This work has several limitations: (1) Although we conduct transfer learning experiments to ImageNet and COCO, the benchmark is mainly focused on CIFAR-100, which may lead to questionable findings for broader downstream tasks. However, all our transfer learning results are consistent with the CIFAR-100 findings. Moreover, our released code can be easily extended to other tasks. Users can thus easily conduct validations with it. (2) BOCB is more complex than current metrics such as parameters and FLOPs, which may lead to inconvenience in practice. We suggest researchers use our code, selecting representative optimizers, such as SGD, Adam, and AdamW, for the ridge plot validation and CIFAR-100 benchmarks, which are practical and resource-efficient. We also call for further explorations of BOCB in the community to advance vision systems together.

ACKNOWLEDGEMENT

We sincerely thank Zhuang Liu for the insightful discussions and valuable suggestions. This work was done by Juanxi Tian, Zedong Wang, and Luyuan Zhang during their internship at Westlake University. And this work was supported by National Key R&D Program of China (No. 2022ZD0115100), National Natural Science Foundation of China Project (No. U21A20427), and Project (No. WU2022A009) from the Center of Synthetic Biology and Integrated Bioengineering of Westlake University. We also thank the AI Station of Westlake University and Alibaba Cloud Computing Co. Ltd. for the support of GPUs.

REFERENCES

- Kai Chen, Jiaqi Wang, Jiangmiao Pang, Yuhang Cao, Yu Xiong, Xiaoxiao Li, Shuyang Sun, Wansen Feng, Ziwei Liu, Jiarui Xu, Zheng Zhang, Dazhi Cheng, Chenchen Zhu, Tianheng Cheng, Qijie Zhao, Buyu Li, Xin Lu, Rui Zhu, Yue Wu, Jifeng Dai, Jingdong Wang, Jianping Shi, Wanli Ouyang, Chen Change Loy, and Dahua Lin. MMDetection: Open mmlab detection toolbox and benchmark. <https://github.com/open-mmlab/mmdetection>, 2019. 16, 18
- Xiangning Chen, Chen Liang, Da Huang, Esteban Real, Kaiyuan Wang, Hieu Pham, Xuanyi Dong, Thang Luong, Cho-Jui Hsieh, Yifeng Lu, and Quoc V Le. Symbolic discovery of optimization algorithms. In *Thirty-seventh Conference on Neural Information Processing Systems*, 2023. 5, 17
- MMPose Contributors. Openmmlab pose estimation toolbox and benchmark. <https://github.com/open-mmlab/mmpose>, 2020. 18
- Ekin D Cubuk, Barret Zoph, Jonathon Shlens, and Quoc V Le. Randaugment: Practical automated data augmentation with a reduced search space. In *Proceedings of the IEEE/CVF Conference on Computer Vision and Pattern Recognition Workshops (CVPRW)*, pp. 702–703, 2020. 5, 16
- Ekin Dogus Cubuk, Barret Zoph, Dandelion Mané, Vijay Vasudevan, and Quoc V. Le. Autoaugment: Learning augmentation strategies from data. *Conference on Computer Vision and Pattern Recognition (CVPR)*, pp. 113–123, 2019. 16
- Xiaohan Ding, X. Zhang, Ningning Ma, Jungong Han, Guiguang Ding, and Jian Sun. Repvgg: Making vgg-style convnets great again. In *Conference on Computer Vision and Pattern Recognition (CVPR)*, pp. 13728–13737, 2021. 5
- Xiaohan Ding, Yiyuan Zhang, Yixiao Ge, Sijie Zhao, Lin Song, Xiangyu Yue, and Ying Shan. Unireplknet: A universal perception large-kernel convnet for audio, video, point cloud, time-series and image recognition. In *Conference on Computer Vision and Pattern Recognition (CVPR)*, 2024. 3, 5, 8
- Alexey Dosovitskiy, Lucas Beyer, Alexander Kolesnikov, Dirk Weissenborn, Xiaohua Zhai, Thomas Unterthiner, Mostafa Dehghani, Matthias Minderer, Georg Heigold, Sylvain Gelly, Jakob Uszkoreit, and Neil Houlsby. An image is worth 16x16 words: Transformers for image recognition at scale. In *International Conference on Learning Representations*, 2021. 1, 2, 3, 6, 16
- John C. Duchi, Elad Hazan, and Yoram Singer. Adaptive subgradient methods for online learning and stochastic optimization. *Journal of Machine Learning Research*, 12:2121–2159, 2011. 4, 5, 17
- Boris Ginsburg, Igor Gitman, and Yang You. Large batch training of convolutional networks with layer-wise adaptive rate scaling. In *International Conference on Learning Representations (ICLR)*, 2018. 5, 17
- Boris Ginsburg, Patrice Castonguay, Oleksii Hrinchuk, Oleksii Kuchaiev, Vitaly Lavrukhin, Ryan Leary, Jason Li, Huyen Nguyen, Yang Zhang, and Jonathan M. Cohen. Stochastic gradient methods with layer-wise adaptive moments for training of deep networks, 2020. 5, 17
- Benjamin Graham, Alaaeldin El-Nouby, Hugo Touvron, Pierre Stock, Armand Joulin, Hervé Jégou, and Matthijs Douze. Levit: a vision transformer in convnet’s clothing for faster inference. In *International Conference on Computer Vision (ICCV)*, pp. 12259–12269, 2021. 16
- Kaiming He, Xiangyu Zhang, Shaoqing Ren, and Jian Sun. Deep residual learning for image recognition. In *Conference on Computer Vision and Pattern Recognition (CVPR)*, pp. 770–778, 2016. 1, 2, 3, 5, 16, 17
- Kaiming He, Georgia Gkioxari, Piotr Dollár, and Ross Girshick. Mask r-cnn. In *International Conference on Computer Vision (ICCV)*, 2017. 1
- Byeongho Heo, Sanghyuk Chun, Seong Joon Oh, Dongyoon Han, Sangdoo Yun, Gyuwan Kim, Youngjung Uh, and Jung-Woo Ha. Adamp: Slowing down the slowdown for momentum optimizers on scale-invariant weights. In *International Conference on Learning Representations*, 2021. 4, 5, 17
- Geoffrey E. Hinton. Adadelata: An adaptive learning rate method. *ArXiv*, 2012. URL https://www.cs.toronto.edu/~hinton/coursera_slides.html. 4, 5, 17

- Jie Hu, Li Shen, and Gang Sun. Squeeze-and-excitation networks. In *Conference on Computer Vision and Pattern Recognition (CVPR)*, pp. 7132–7141, 2018. 16
- Gao Huang, Yu Sun, Zhuang Liu, Daniel Sedra, and Kilian Q. Weinberger. Deep networks with stochastic depth. In *European Conference on Computer Vision (ECCV)*, 2016. 5, 17
- Gao Huang, Zhuang Liu, and Kilian Q. Weinberger. Densely connected convolutional networks. In *Conference on Computer Vision and Pattern Recognition (CVPR)*, pp. 2261–2269, 2017. 5, 16
- Diederik P. Kingma and Jimmy Ba. Adam: A method for stochastic optimization. In *International Conference on Learning Representations (ICLR)*, 2015. 1, 4, 5, 17
- Alexander Kirillov, Eric Mintun, Nikhila Ravi, Hanzi Mao, Chloe Rolland, Laura Gustafson, Tete Xiao, Spencer Whitehead, Alexander C. Berg, Wan-Yen Lo, Piotr Dollár, and Ross B. Girshick. Segment anything. In *International Conference on Computer Vision (ICCV)*, pp. 3992–4003, 2023. 1
- Alex Krizhevsky, Geoffrey Hinton, et al. Learning multiple layers of features from tiny images. 2009. 1, 5, 16, 18
- Alex Krizhevsky, Ilya Sutskever, and Geoffrey E Hinton. Imagenet classification with deep convolutional neural networks. In F. Pereira, C.J. Burges, L. Bottou, and K.Q. Weinberger (eds.), *Advances in Neural Information Processing Systems*. Curran Associates, Inc., 2012a. 1, 3, 5
- Alex Krizhevsky, Ilya Sutskever, and Geoffrey E. Hinton. Imagenet classification with deep convolutional neural networks. *Communications of the ACM*, 60:84 – 90, 2012b. 1, 10, 16
- Siyuan Li, Zedong Wang, Zicheng Liu, Di Wu, and Stan Z. Li. Openmixup: Open mixup toolbox and benchmark for visual representation learning. <https://github.com/Westlake-AI/openmixup>, 2022. 16
- Siyuan Li, Zedong Wang, Zicheng Liu, Cheng Tan, Haitao Lin, Di Wu, Zhiyuan Chen, Jiangbin Zheng, and Stan Z. Li. Moganet: Multi-order gated aggregation network. In *International Conference on Learning Representations (ICLR)*, 2024. 5, 8, 18
- Tsung-Yi Lin, Michael Maire, Serge Belongie, James Hays, Pietro Perona, Deva Ramanan, Piotr Dollár, and C Lawrence Zitnick. Microsoft coco: Common objects in context. In *European Conference on Computer Vision (ECCV)*, pp. 740–755. Springer, 2014. 1, 16, 18
- Tsung-Yi Lin, Priya Goyal, Ross Girshick, Kaiming He, and Piotr Dollár. Focal loss for dense object detection. In *International Conference on Computer Vision (ICCV)*, 2017. 11, 18
- Hong Liu, Zhiyuan Li, David Hall, Percy Liang, and Tengyu Ma. Sophia: A scalable stochastic second-order optimizer for language model pre-training, 2023. 5, 17
- Liyuan Liu, Haoming Jiang, Pengcheng He, Weizhu Chen, Xiaodong Liu, Jianfeng Gao, and Jiawei Han. On the variance of the adaptive learning rate and beyond. In *International Conference on Learning Representations*, 2020. 5, 17
- Ze Liu, Yutong Lin, Yue Cao, Han Hu, Yixuan Wei, Zheng Zhang, Stephen Lin, and Baining Guo. Swin transformer: Hierarchical vision transformer using shifted windows. In *International Conference on Computer Vision (ICCV)*, pp. 9992–10002, 2021. 3, 5, 16, 17, 18
- Zhuang Liu, Hanzi Mao, Chao-Yuan Wu, Christoph Feichtenhofer, Trevor Darrell, and Saining Xie. A convnet for the 2020s. In *Conference on Computer Vision and Pattern Recognition (CVPR)*, 2022a. 1, 2, 5, 6, 8, 17
- Zicheng Liu, Siyuan Li, Di Wu, Zhiyuan Chen, Lirong Wu, Jianzhu Guo, and Stan Z. Li. Automix: Unveiling the power of mixup for stronger classifiers. In *European Conference on Computer Vision (ECCV)*, 2022b. 17
- Ilya Loshchilov and Frank Hutter. Sgdr: Stochastic gradient descent with warm restarts. *arXiv preprint arXiv:1608.03983*, 2016. 16
- Ilya Loshchilov and Frank Hutter. Decoupled weight decay regularization. In *International Conference on Learning Representations (ICLR)*, 2019. 1, 2, 5, 17

- Liangchen Luo, Yuanhao Xiong, and Yan Liu. Adaptive gradient methods with dynamic bound of learning rate. In *International Conference on Learning Representations*, 2019. 4, 5, 17
- Charles H. Martin and Michael W. Mahoney. Implicit self-regularization in deep neural networks: Evidence from random matrix theory and implications for learning. *Journal of Machine Learning Research*, 22(165):1–73, 2021. 19
- Charles H Martin, Tongsu Peng, and Michael W Mahoney. Predicting trends in the quality of state-of-the-art neural networks without access to training or testing data. *Nature Communications*, 12(1):4122, 2021. 2, 5, 8, 9, 11, 19
- Microsoft. Neural Network Intelligence, 1 2021. URL <https://github.com/microsoft/nni>. 5, 18
- Maxime Oquab, Timothée Darcet, Théo Moutakanni, Huy Q. Vo, Marc Szafraniec, Vasil Khalidov, Pierre Fernandez, Daniel Haziza, Francisco Massa, Alaaeldin El-Nouby, Mahmoud Assran, Nicolas Ballas, Wojciech Galuba, Russ Howes, Po-Yao (Bernie) Huang, Shang-Wen Li, Ishan Misra, Michael G. Rabbat, Vasu Sharma, Gabriel Synnaeve, Huijiao Xu, Hervé Jégou, Julien Mairal, Patrick Labatut, Armand Joulin, and Piotr Bojanowski. Dinov2: Learning robust visual features without supervision. *ArXiv*, abs/2304.07193, 2023. 1
- Boris Polyak and Anatoli B. Juditsky. Acceleration of stochastic approximation by averaging. *Siam Journal on Control and Optimization*, 30:838–855, 1992. 17
- Sashank J. Reddi, Satyen Kale, and Surinder Kumar. On the convergence of adam and beyond. In *International Conference on Learning Representations*, 2018. 4, 5, 17
- Shaoqing Ren, Kaiming He, Ross B. Girshick, and Jian Sun. Faster r-cnn: Towards real-time object detection with region proposal networks. *IEEE Transactions on Pattern Analysis and Machine Intelligence (TPAMI)*, 39:1137–1149, 2015. 16
- Mark Sandler, Andrew G. Howard, Menglong Zhu, Andrey Zhmoginov, and Liang-Chieh Chen. Mobilenetv2: Inverted residuals and linear bottlenecks. In *Conference on Computer Vision and Pattern Recognition (CVPR)*, pp. 4510–4520, 2018. 2, 3, 5
- Noam M. Shazeer. Glu variants improve transformer. *ArXiv*, abs/2002.05202, 2020. 16
- Noam M. Shazeer and Mitchell Stern. Adafactor: Adaptive learning rates with sublinear memory cost. *ArXiv*, abs/1804.04235, 2018. 4, 5, 17
- Sam Shleifer, Jason Weston, and Myle Ott. Normformer: Improved transformer pretraining with extra normalization. *ArXiv*, 2021. 7, 16
- Karen Simonyan and Andrew Zisserman. Very deep convolutional networks for large-scale image recognition. In *International Conference on Learning Representations (ICLR)*, 2015. 1, 2, 5
- Naresh K. Sinha and Michael P. Griscik. A stochastic approximation method. *IEEE Transactions on Systems, Man, and Cybernetics*, SMC-1(4):338–344, Oct 1971. 1, 2, 4, 5, 17
- Christian Szegedy, Wei Liu, Yangqing Jia, Pierre Sermanet, Scott Reed, Dragomir Anguelov, Dumitru Erhan, Vincent Vanhoucke, and Andrew Rabinovich. Going deeper with convolutions. In *Conference on Computer Vision and Pattern Recognition (CVPR)*, pp. 1–9, 2015. 16
- Christian Szegedy, Vincent Vanhoucke, Sergey Ioffe, Jonathon Shlens, and Zbigniew Wojna. Rethinking the inception architecture for computer vision. In *Conference on Computer Vision and Pattern Recognition (CVPR)*, pp. 2818–2826, 2016. 5, 16, 17
- Mingxing Tan and Quoc Le. Efficientnet: Rethinking model scaling for convolutional neural networks. In *International conference on machine learning (ICML)*, pp. 6105–6114. PMLR, 2019. 2, 5
- Ilya O. Tolstikhin, Neil Houlsby, Alexander Kolesnikov, Lucas Beyer, Xiaohua Zhai, Thomas Unterthiner, Jessica Yung, Daniel Keysers, Jakob Uszkoreit, Mario Lucic, and Alexey Dosovitskiy. Mlp-mixer: An all-mlp architecture for vision. In *Advances in Neural Information Processing Systems (NeurIPS)*, 2021. 2, 5

- Hugo Touvron, Matthieu Cord, Matthijs Douze, Francisco Massa, Alexandre Sablayrolles, and Herve Jegou. Training data-efficient image transformers & distillation through attention. In *International Conference on Machine Learning (ICML)*, pp. 10347–10357, 2021a. 5, 16, 17
- Hugo Touvron, Matthieu Cord, Alexandre Sablayrolles, Gabriel Synnaeve, and Hervé Jégou. Going deeper with image transformers. In *International Conference on Computer Vision (ICCV)*, pp. 32–42, 2021b. 7, 16
- Kirill Vishniakov, Zhiqiang Shen, and Zhuang Liu. Convnet vs transformer, supervised vs clip: Beyond imagenet accuracy. *ArXiv*, abs/2311.09215, 2023. 1
- Qiang Wang, Bei Li, Tong Xiao, Jingbo Zhu, Changliang Li, Derek F. Wong, and Lidia S. Chao. Learning deep transformer models for machine translation. In *Annual Meeting of the Association for Computational Linguistics*, 2019. 16
- Ross Wightman, Hugo Touvron, and Hervé Jégou. Resnet strikes back: An improved training procedure in timm, 2021. 17
- Sanghyun Woo, Jongchan Park, Joon-Young Lee, and In-So Kweon. Cbam: Convolutional block attention module. In *European Conference on Computer Vision (ECCV)*, 2018. 3
- Sanghyun Woo, Shoubhik Debnath, Ronghang Hu, Xinlei Chen, Zhuang Liu, In-So Kweon, and Saining Xie. Convnext v2: Co-designing and scaling convnets with masked autoencoders. In *Conference on Computer Vision and Pattern Recognition (CVPR)*, 2023. 1, 5, 8
- Bin Xiao, Haiping Wu, and Yichen Wei. Simple baselines for human pose estimation and tracking. In *European Conference on Computer Vision (ECCV)*, 2018. 18
- Xingyu Xie, Pan Zhou, Huan Li, Zhouchen Lin, and Shuicheng YAN. Adan: Adaptive nesterov momentum algorithm for faster optimizing deep models. *IEEE Transactions on Pattern Analysis and Machine Intelligence*, 2023. 5, 17
- Yang You, Jing Li, Sashank Reddi, Jonathan Hseu, Sanjiv Kumar, Srinadh Bhojanapalli, Xiaodan Song, James Demmel, Kurt Keutzer, and Cho-Jui Hsieh. Large batch optimization for deep learning: Training BERT in 76 minutes. In *International Conference on Learning Representations (ICLR)*, 2020. 5, 17
- Weihao Yu, Pan Zhou, Shuicheng Yan, and Xinchao Wang. Inceptionnext: When inception meets convnext. *ArXiv*, abs/2303.16900, 2023. 8
- Weihao Yu, Chenyang Si, Pan Zhou, Mi Luo, Yichen Zhou, Jiashi Feng, Shuicheng Yan, and Xinchao Wang. Metaformer baselines for vision. *IEEE Transactions on Pattern Analysis and Machine Intelligence*, 46:896–912, 2024. 1, 2, 3, 5
- Sangdoo Yun, Dongyoon Han, Seong Joon Oh, Sanghyuk Chun, Junsuk Choe, and Youngjoon Yoo. Cutmix: Regularization strategy to train strong classifiers with localizable features. In *International Conference on Computer Vision (ICCV)*, pp. 6023–6032, 2019. 17
- Matthew D. Zeiler. Neural networks for machine learning. *ArXiv*, abs/1212.5701, 2012. 5, 17
- Hang Zhang, Chongruo Wu, Zhongyue Zhang, Yi Zhu, Haibin Lin, Zhi Zhang, Yue Sun, Tong He, Jonas Mueller, R Manmatha, et al. Resnest: Split-attention networks. In *Conference on Computer Vision and Pattern Recognition (CVPR)*, pp. 2736–2746, 2022. 2
- Hongyi Zhang, Moustapha Cisse, Yann N Dauphin, and David Lopez-Paz. mixup: Beyond empirical risk minimization. In *International Conference on Learning Representations (ICLR)*, 2018. 5, 17
- Zhun Zhong, Liang Zheng, Guoliang Kang, Shaozi Li, and Yi Yang. Random erasing data augmentation. In *AAAI Conference on Artificial Intelligence (AAAI)*, pp. 13001–13008, 2020. 17
- Juntang Zhuang, Tommy Tang, Yifan Ding, Sekhar C Tatikonda, Nicha Dvornek, Xenophon Papademetris, and James Duncan. Adabelief optimizer: Adapting stepsizes by the belief in observed gradients. In H. Larochelle, M. Ranzato, R. Hadsell, M.F. Balcan, and H. Lin (eds.), *Advances in Neural Information Processing Systems*, volume 33, pp. 18795–18806. Curran Associates, Inc., 2020. 5, 17

SUPPLEMENT MATERIAL

The appendix sections are structured as follows:

- In Appendix A, we provide experimental setups for benchmarks, including information on backbones and optimizers, training recipes, and hyperparameter settings.
- In Appendix B, we provide full experimental results and analysis of the proposed benchmarks.
- In Appendix C, we visualize the learned parameters and explain the BOCB effects.

A IMPLEMENTATION DETAILS

This section provides experimental settings of benchmarks and dataset information for Sec 3. As shown in Table A1, we summarize 16 typical vision networks proposed into three categories as discussed in Sec. 2.1, where typical and useful techniques are listed and the training settings are provided in Table A3. As for benchmark settings, we apply consistent setups for image classification tasks on CIFAR-100 (Krizhevsky et al., 2009) and ImageNet-1K (Krizhevsky et al., 2012b) based on OpenMixup (Li et al., 2022) codebase with 1 or 8 Nvidia A100 GPUs, while employing object detection and pose estimation tasks (Ren et al., 2015) on COCO (Lin et al., 2014) with MMLab codebases (Chen et al., 2019). Table A2 shows detailed information on categories of 20 widely adopted optimizers.

Table A1: Three categories of typical vision backbones proposed in the past decade. For operators in different network blocks, Conv, SepConv, and DWConv denote normal convolutions, separable convolution, and depth-wise convolution, Gating denotes GLU-like modules (Shazeer, 2020), and SE denotes Squeeze-and-excitation block (Hu et al., 2018). As for the design of residual connection and normalization, the vanilla residual branch use addition (He et al., 2016) or concatenation (Huang et al., 2017), PreNorm denotes the pre-act normalization (Wang et al., 2019) with residual connection, LayerScale (Touvron et al., 2021b) and ResScale (Shleifer et al., 2021) are layer-wise initialization tricks for stabilize training of deep models.

Backbone	Date	Stage-wise design	Block-wise design	Operator (feature extractor)	Residual branch	Input size	Training setting
AlexNet	NeurIPS'2012	-	Plain	Conv	-	224	PyTorch
VGG	ICLR'2015	-	Plain	Conv	-	224	PyTorch
ResNet	CVPR'2016	Hierarchical	Bottleneck	Conv	Addition	32	PyTorch
DenseNet	CVPR'2017	Hierarchical	Bottleneck	Conv	Concatenation	32	PyTorch
MobileNet_V2	CVPR'2018	Hierarchical	Inv-bottleneck	SepConv	Addition	224	PyTorch
EfficientNet	ICML'2019	Hierarchical	Inv-bottleneck	Conv & SE	Addition	224	RSB A2
RepVGG	CVPR'2021	Hierarchical	Inv-bottleneck	Conv	Addition	224	PyTorch
DeiT-S (ViT)	ICML'2021	Patchfy & Isotropic	Metaformer	Attention	PreNorm	224	DeiT
MLP-Mixer	NeurIPS'2021	Patchfy & Isotropic	Metaformer	MLP	PreNorm	224	DeiT
Swin Transformer	ICCV'2021	Patchfy & Hierarchical	Metaformer	Local Attention	PreNorm	224	ConvNeXt
ConvNeXt	CVPR'2022	Patchfy & Hierarchical	MetaNeXt	DWConv	PreNorm & LayerScale	32	ConvNeXt
ConvNeXt_V2	CVPR'2023	Patchfy & Hierarchical	MetaNeXt	DWConv	PreNorm & LayerScale	32	ConvNeXt
MogaNet	ICLR'2024	Patchfy & Hierarchical	Metaformer	DWConv & Gating	PreNorm & LayerScale	32	ConvNeXt
UniRepLKNet	CVPR'2024	Patchfy & Hierarchical	Metaformer	DWConv & SE	PreNorm & LayerScale	224	ConvNeXt
TransNeXt	CVPR'2024	Patchfy & Hierarchical	Metaformer	Attention & Gating	PreNorm & LayerScale	224	DeiT
IdentityFormer	TPAMI'2024	Patchfy & Hierarchical	Metaformer	Identity	PreNorm & ResScale	224	RSB A2
PoolFormerV2	TPAMI'2024	Patchfy & Hierarchical	Metaformer	Pooling	PreNorm & ResScale	224	RSB A2
ConvFormer	TPAMI'2024	Patchfy & Hierarchical	Metaformer	SepConv	PreNorm & ResScale	224	RSB A2
AttentionFormer	TPAMI'2024	Patchfy & Hierarchical	Metaformer	Attention	PreNorm & ResScale	224	RSB A2
CAFormer	TPAMI'2024	Patchfy & Hierarchical	Metaformer	SepConv & Attention	PreNorm & ResScale	224	RSB A2

A.1 IMAGE CLASSIFICATION

ImageNet-1K. Following the widely used modern training recipes, we consider three regular training settings for ImageNet-1K (Krizhevsky et al., 2012b) classification experiments for various backbones and optimizers, which could be transplanted to the proposed CIFAR-100 benchmarks. As shown in Table A3, these training schemes include data preprocessing and augmentations, optimizing setups, regularization tricks, and loss functions: (1) Classical **PyTorch-style setting** (Szegedy et al., 2016) applies basic data augmentations, RandomResizeCrop (or RandomCrop for 32² resolutions), HorizontalFlip, and CenterCrop (Szegedy et al., 2015), basic SGD training setups with cosine learning rate scheduler (Loshchilov & Hutter, 2016), and the cross-entropy (CE) loss. (2) **DeiT and ConvNeXt settings** (Touvron et al., 2021a; Liu et al., 2021) are designed for Transformer and modern CNN architectures like ViTs (Dosovitskiy et al., 2021; Graham et al., 2021), which utilizes several advanced augmentations (Cubuk et al., 2019) (like RandAugment (Cubuk

Table A2: Four categories of typical optimizers with their components. From top to bottom are (a) fixed learning rate with momentum gradient, (b) adaptive learning rate with momentum gradient, (c) estimated learning rate with momentum gradient, and (d) adaptive learning rate with current gradient.

Optimizer	Date	Learning rate	Gradient	Weight decay
SGD-M (Sinha & Griscik, 1971)	TSMC'1971	Fixed lr	Momentum	✓
SGDP (Heo et al., 2021)	ICLR'2021	Fixed lr	Momentum	Decoupled
LION (Chen et al., 2023)	NIPS'2023	Fixed lr	Sign Momentum	Decoupled
Adam (Kingma & Ba, 2015)	ICLR'2015	Estimated second moment	Momentum	✓
Adamax (Kingma & Ba, 2015)	ICLR'2015	Estimated second moment	Momentum	✓
AdamW (Loshchilov & Hutter, 2019)	ICLR'2019	Estimated second moment	Momentum	Decoupled
AdamP (Heo et al., 2021)	ICLR'2021	Estimated second moment	Momentum	Decoupled
LAMB (You et al., 2020)	ICLR'2020	Estimated second moment	Momentum	Decoupled
NAdam (Reddi et al., 2018)	ICLR'2018	Estimated second moment	Nesterov Momentum	✓
RAdam (Liu et al., 2020)	ICLR'2020	Estimated second moment	Momentum	Decoupled
Adan (Xie et al., 2023)	TPAMI'2023	Estimated second moment Nesterov	Momentum	Decoupled
AdaBelief (Zhuang et al., 2020)	NIPS'2019	Estimated second moment variance	Momentum	Decoupled
AdaBound (Luo et al., 2019)	ICLR'2019	Estimated second moment	Momentum	Decoupled
AdaFactor (Shazeer & Stern, 2018)	ICML'2018	Estimated second moment (decomposition)	Momentum	Decoupled
LARS (Ginsburg et al., 2018)	ICLR'2018	L2-norm of Gradient	Momentum	Decoupled
Novograd (Ginsburg et al., 2020)	arXiv'2020	Sum of estimated second momentum	Momentum	Decoupled
Sophia (Liu et al., 2023)	arXiv'2023	Parameter-based estimator	Sign Momentum	Decoupled
AdaGrad (Duchi et al., 2011)	JMLR'2011	Second moment	Gradient	✓
AdaDelta (Zeiler, 2012)	arXiv'2012	Estimated second moment param moment	Gradient	✓
RMSProp (Hinton, 2012)	arXiv'2012	Estimated second moment	Gradient	✓

et al., 2020), Mixup (Zhang et al., 2018) and CutMix (Yun et al., 2019; Liu et al., 2022b), Random Erasing (Zhong et al., 2020), ColorJitter (He et al., 2016)), and regularization techniques (Stochastic Depth (Huang et al., 2016), Label Smoothing (Szegedy et al., 2016), and EMA (Polyak & Juditsky, 1992). (3) **RSB A2/A3 settings** (Wightman et al., 2021) are designed for CNNs to boost their performance and convergence speeds as ViTs, which reduces the augmentation strengths and replaces the CE loss with Binary Cross Entropy (BCE) loss compared to the DeiT setting. The optimizing hyper-parameters marked in gray, like initial learning rate, optimizer momentum, and weight decay, will be tuned based on the optimizer. We use the threshold $\lambda = 1$ in Eq. (1) to discriminate BOCB results on ImageNet-1K.

Table A3: Ingredients and hyper-parameters used for image classification training settings. Taking ImageNet-1K as the template setups, the settings of PyTorch (Szegedy et al., 2016) and RSB A2/A3 (Wightman et al., 2021) take ResNet-50 (He et al., 2016) as the examples, the DeiT (Touvron et al., 2021a) setting takes DeiT-S as the example, and the ConvNeXt (Liu et al., 2022a) setting is a variant of the DeiT setting for ConvNeXt and Swin Transformer (Liu et al., 2021). Gray regions should be modified for each optimizer.

Procedure	PyTorch		DeiT		ConvNeXt	RSB A2		RSB A3
Dataset	IN-1K	CIFAR	IN-1K	CIFAR	CIFAR	IN-1K	CIFAR	IN-1K
Train Resolution	224	224	224	224	32	224	224	160
Test Resolution	224	224	224	224	32	224	224	224
Test crop ratio	0.875	1.0	0.875	1.0	1.0	0.95	1.0	0.95
Epochs	100	200	300	200	200	300	200	100
Batch size	256	100	1024	100	100	2048	100	2048
Optimizer	SGD		AdamW		AdamW	LAMB		LAMB
Learning rate	0.1		1×10^{-3}		1×10^{-3}	5×10^{-3}		8×10^{-3}
Optimizer Momentum	0.9		0.9, 0.999		0.9, 0.999	0.9, 0.999		0.9, 0.999
Weight decay	10^{-4}		0.05		0.05	0.02		0.02
LR decay	Cosine		Cosine		Cosine	Cosine		Cosine
Warmup epochs	X		5		20	5		5
Label smoothing ϵ	X		0.1		0.1	X		X
Dropout	X		X		X	X		X
Stochastic Depth	X		0.1		0.1	0.05		X
Repeated Augmentation	X		✓		✓	✓		X
Gradient Clip.	X		5.0		X	X		X
Horizontal flip	✓		✓		✓	✓		✓
RandomResizedCrop	✓		✓		✓	✓		✓
Rand Augment	X		9/0.5		9/0.5	7/0.5		6/0.5
Auto Augment	X		X		X	X		X
Mixup α	X		0.8		0.8	0.1		0.1
Cutmix α	X		1.0		1.0	1.0		1.0
Erasing probability	X		0.25		0.25	X		X
ColorJitter	X		X		X	X		X
EMA	X		✓		✓	X		X
CE loss	✓		✓		✓	X		X
BCE loss	X		X		X	✓		✓

CIFAR-100. Inheriting the training settings on ImageNet-1K, we modify the input resolutions and batch size to build the corresponding settings for CIFAR-100 (Krizhevsky et al., 2009) benchmarks. The original CIFAR-100 dataset contains 50k training images and 10k testing images in 32^2 resolutions, and we consider two input resolutions. As shown in Table A3, in the case of 32^2 resolutions, the downsampling ratio of the first stem in CNNs will be set to $\frac{1}{2}$; in the case of 224^2 resolutions (cubic upsampling to 224^2), the backbone structure keep the same as on ImageNet-1K. We use different training settings for a fair comparison of classical CNNs and modern Transformers on CIFAR-100, which contains 50k training images and 10k testing images of 32^2 resolutions. As for classical CNNs with bottleneck structures, we use 32^2 resolutions with the CIFAR version of network architectures, *i.e.*, downsampling the input size to $\frac{1}{2}$ in the stem module instead of $\frac{1}{8}$ on ImageNet-1K. All the benchmarked backbones are trained for 200 epochs from the stretch. We set $\lambda = 3$ in Eq. (1) to discriminate BOCB results on CIFAR-100.

Optimizing hyper-parameters search. For a fair comparison, we only search two common hyper-parameters (the learning rate and weight decay) heuristically with NNI toolbox (Microsoft, 2021), *i.e.*, determining the NNI search range of hyper-parameters manually. We regard each hyper-parameter as a set of discrete values, choosing 5 consecutive values centered on the heuristically determined initial value. As for the specific hyper-parameters of some optimizers, *e.g.*, ϵ for AdaBelief and the final lr for AdaBound, we further search for their optimal values separately. Table A1 shows the training setting for each backbone. The basis hyper-parameters of various optimizers for different vision backbones on CIFAR-100 are provided in the supplementary material.

A.2 OBJECT DETECTION AND POSE ESTIMATION

Object Detection. Following Swin Transformers (Liu et al., 2021), we first evaluate objection detection as the representative vision downstream task on COCO (Lin et al., 2014) for transfer learning, which includes 118K training images (*train2017*) and 5K validation images (*val2017*). Experiments of COCO detection and segmentations are implemented on MMDetection (Chen et al., 2019) codebase and run on 4 Tesla V100 GPUs. Taking RetinaNet (Lin et al., 2017) as the standard detector, the original fine-tuning setting for ResNet-50 employs the SGD optimizer with $1 \times$ (12 epochs) training with a batch size of 16 and a fixed step learning rate scheduler. As for Swin-T, the official setting employs the AdamW optimizer with $1 \times$ scheduler and a batch size of 16. During training, the shorter side of training images is resized to 800 pixels, and the longer side is resized to not more than 1333 pixels. For different pre-trained models (PyTorch, DeiT, and RSB A2/A3 pre-training), we search basic hyper-parameters (the learning rate and the weight decay) for every optimizer as described in Sec. A.1 to get relatively optimal results. We set $\lambda = 3$ in Eq. (1) to discriminate BOCB results for objection detection.

2D Pose Estimation. We also evaluate transfer learning to 2D human key-points estimation task on COCO based on Top-Down SimpleBaseline (Xiao et al., 2018) (adding a Top-Down estimation head after the backbone) following MogaNet (Li et al., 2024). The original training setting is to fine-tune the pre-trained backbone and the randomly initialized head for 210 epochs with Adam optimizer with a multi-step learning rate scheduler decay at 170 and 200 epochs. We also search learning rates and weight decays for all optimizers. The training and testing images are resized to 256×192 or 384×288 resolutions, and these experiments are implemented with MMPose (Contributors, 2020) codebase and run on 4 Tesla V100 GPUs. We set $\lambda = 3$ in Eq. (1) to discriminate BOCB results for the pose estimation task.

A.3 EMPIRICAL ANALYSIS

To gain deeper insights into the observed *backbone-optimizer coupling bias* (BOCB) phenomenon, we conducted a collection of empirical analysis focusing on two key aspects: hyper-parameter stability and model parameter patterns. These analyses provide valuable information about the intrinsic properties of different network architectures and their interactions with various optimizers.

Hyper-parameter stability. We developed an approach to quantify the hyper-parameter stability of vision backbones and optimizers, which serves as a proxy for understanding the strength of backbone-optimizer coupling. This analysis involves the following steps: (1) Optimal Settings Identification: For each backbone-optimizer pair, we conducted extensive grid searches to identify the optimal hyper-parameters (learning rate and weight decay). (2) One-hot Encoding: We converted these optimal hyper-parameters into discrete one-hot encoded vectors. Assuming n possible learning rates and m

possible weight decays, we created vectors $\{\tilde{r}_i\}_{i=1}^n$ and $\{\tilde{\omega}_i\}_{i=1}^m$. (3) Mode Statistics: We computed histogram-based mode (most common) statistics M_r and M_ω across all optimizers for each backbone. (4) Variation Computation: We quantified the *variation* between each hyper-parameter and mode statistics using the Manhattan distance, $\sum_{i=1}^n |\tilde{r}_i - M_r| + \sum_{i=1}^m |\tilde{\omega}_i - M_\omega|$. (5) Visualization: We plot the distribution of these variations for both backbones (Figure 4) and optimizers (Figure 5), which offer intuitive insights into the relative stability and adaptability of different backbone-optimizer pairs. As for backbones, lower variation indicates higher stability and potentially weaker coupling bias, as the backbone performs well across a range of optimizers with similar hyper-parameters. For the optimizers, lower variation suggests better generalizability across different network architectures.

Patterns of learned parameters. To investigate the layer-wise properties discussed in Section 2.1, we employed a set of quantitative metrics to analyze the learned parameters of each layer. As shown in Section C, these metrics reveal intrinsic topological patterns that reflect the unique characteristics of different network architectures, such as stage-wise macro designs, building block structures, and core operators of token-mixers and channel-mixers. We focused on the three key indicators as follows:

- **PL Exponent Alpha:** In the context of WeightWatcher (Martin & Mahoney, 2021; Martin et al., 2021), the Power Law (PL) exponent α quantifies the learned parameter quality of neural network layers. It is extracted from the tail fit of the layer weight matrix’s Empirical Spectral Density (ESD) to a truncated Power Law: $\rho(\lambda) \sim \lambda^{-\alpha}$, $\rho(\lambda)$ denotes the ESD, and λ represents the eigenvalues of the weight matrix’s correlation matrix $X = W^T W$. The exponent α reflects the correlation structure, with lower values indicating enhanced generalization capabilities, and higher values suggesting potential overfitting or underfitting. This metric facilitates the assessment of neural network models’ generalization tendencies without the need for training or testing datasets, serving as an intrinsic measure of model quality.
- **Entropy:** The information entropy of the learned parameter tensor, $H = -\sum p_i \log(p_i)$, where p_i is the probability of each value in the parameter tensor. It is used to measure the randomness of the parameter distribution. Higher entropy indicates a more uniform or random distribution, while lower entropy suggests a more patterned distribution. This provides insights into the complexity and information of each layer, helping to identify layers with more structured weight distributions.
- **L_2 -norm:** Euclidean norm (magnitude) of the learned parameter vector $\|w\|_2 = \sqrt{\sum w_i^2}$, where w_i are individual parameters. This reflects the scale of the learned weight matrix and identifies layers with potential dominant effects on the network’s behavior (more influence on the layer output), which could be crucial for understanding the learning results of diverse network architectures.
- **Top- k PCA Energy Ratio:** Cumulative energy ratio of the top- k principal components of the parameter matrix $E_k = (\sum_{i=1}^k \lambda_i) / (\sum_{i=1}^n \lambda_i)$, where λ_i are eigenvalues of the covariance matrix. It measures the concentration of information in the learned parameter matrix. A larger top- k energy indicates that the parameter matrix has more concentrated components. This analysis provides insights into the dimensionality and compressibility of each layer’s parameters, which could be helpful for model pruning and efficiency optimization.

These metrics, when analyzed across different layers and backbone-optimizer combinations, reveal characteristic patterns that correspond to specific architecture designs. We provide ridge plots (as shown in Section C) to visualize these metrics across different layers for various backbone-optimizer combinations. For instance, we may observe distinct entropy patterns in hierarchical vs. isotropic stage-wise architectures, variations in L_2 -norm across different stages of the network, or changes in PCA energy ratios for different types of layers (e.g., convolutional vs. attention-based).

By analyzing these patterns, we can gain valuable insights into how different neural network architectures interact with various optimizers, furthering our understanding of the BOCB phenomenon and informing future design choices for both vision backbones and optimizers.

B FULL EXPERIMENTAL RESULTS

This appendix section provides a detailed expansion of the experimental findings from the main manuscript, specifically aimed at validating the BOCB phenomenon. The results are structured to facilitate a thorough evaluation across the CIFAR-100 and ImageNet-1K datasets, involving a diverse range of both modern and classical vision backbones, each paired with various optimizers. This comprehensive analysis is intended to clarify the complex interactions between neural network architectures and optimization strategies, emphasizing their critical impact on model performance.

and adaptability. Additionally, these insights are applied to practical tasks, such as object detection and pose estimation on COCO, demonstrating the practical relevance of BOCB.

B.1 CIFAR-100 CLASSIFICATION EXPERIMENTS

Our in-depth exploration of the CIFAR-100 dataset was designed to scrutinize the interdependence between network architectures and optimizers. Table 1 encapsulates the top-1 classification accuracy for an extensive lineup of 15 vision backbones, categorized into primary CNNs, classical CNNs, and modern DNNs. The results underscore a pronounced divergence in the optimal optimizer for different architectural eras. Classic architectures such as AlexNet, VGG, and the ResNet family reveal an affinity for SGD-M and SGDP, with these optimizers yielding the most accurate outcomes. This preference indicates a tight coupling between classical CNNs and SGD-based methods. In stark contrast, modern architectures like Vision Transformers, ConvNeXt, and MetaFormer variants thrive under the adaptive learning rates afforded by optimizers such as AdamW, AdamP, and LAMB, showcasing a more flexible coupling bias. To elucidate the nuances of BOCB, we present a hyperparameter sensitivity analysis. This analysis visualizes the distribution of optimal learning rates and weight decays for the evaluated optimizers, as depicted in Figures 3 and 4. Classical CNNs display a concentrated distribution, pointing to a specific hyperparameter set for SGD optimizers. In contrast, modern DNNs exhibit a broader distribution, suggesting a higher tolerance to hyperparameter variations and a more adaptable coupling with a range of optimizers.

B.2 IMAGENET-1K CLASSIFICATION EXPERIMENTS

To ascertain the generalizability of our observations, we extended our evaluation on ImageNet-1K. Table 2 details the Top-1 accuracy for a curated selection of vision backbones under various optimizers. The results are congruent with those from CIFAR-100, reinforcing the BOCB phenomenon. ResNets and EfficientNets continue demonstrating their predilection for SGD-M and SGDP, achieving peak performance with these optimizers. On the other hand, modern DNNs like Vision Transformers and ConvNeXt once again manifest their superiority when paired with AdamW, AdamP, and LAMB, aligning with the adaptive learning rate optimizers' capacity to navigate the complex optimization landscapes of contemporary architectures.

B.3 COCO OBJECT DETECTION AND POSE ESTIMATION EXPERIMENTS

Expanding our analysis from CIFAR-100 and ImageNet-1K, we investigated the BOCB in practical tasks using COCO for object detection and pose estimation. These experiments aimed to assess BOCB's impact on model transferability and task performance when pre-trained models are adapted to specific tasks. In object detection, employing the RetinaNet framework with ImageNet-1K pre-trained models, we observed in Table 3 that backbones trained with adaptive optimizers like AdamW, AdamP, and LAMB achieved higher top-1 accuracies on ImageNet-1K and superior performance on COCO object detection. This suggests that these optimizers enhance feature learning and generalization in downstream tasks by effectively navigating complex optimization landscapes during pre-training.

Similarly, for pose estimation using the TopDown approach, models pre-trained with AdamW, AdamP, and LAMB showed improved performance on COCO, as evidenced by higher AP50 scores in Table 3. This supports the significant influence of the optimizer choice during pre-training on a model's capacity to acquire and transfer knowledge. Our hyperparameter sensitivity analysis, extended to COCO experiments, provides further insights. Figures ?? illustrate the distribution of optimal learning rates and weight decays for various optimizers, revealing that while classical backbones have a narrow optimal range, modern architectures display broader tolerance, reflecting their adaptability to different optimizer settings. This adaptability is crucial for effective transfer learning and task-specific performance.

In summary, the comprehensive experimental results presented in this section provide compelling evidence for the backbone-optimizer coupling bias phenomenon across multiple benchmark datasets and vision tasks. These findings highlight the importance of considering the interplay between network architectures and optimization algorithms when designing and deploying vision systems, as overlooking BOCB can lead to suboptimal performance and potential inefficiencies.

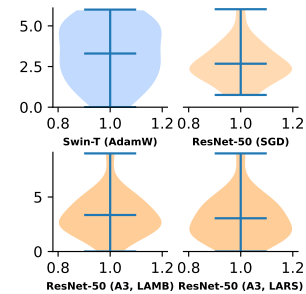


Figure A1: **Violinplot** of hyper-parameters for the aspects of backbones or optimizers on COCO.

C EMPIRICAL EXPERIMENTS

This section delineates a series of empirical experiments meticulously designed to validate the theoretical insights into the BOCB and to elucidate the nuances of this phenomenon within the context of network architecture and optimization strategies. The experiments are crafted to furnish a comprehensive understanding of BOCB, its implications for vision backbones, and its interaction with various optimization techniques.

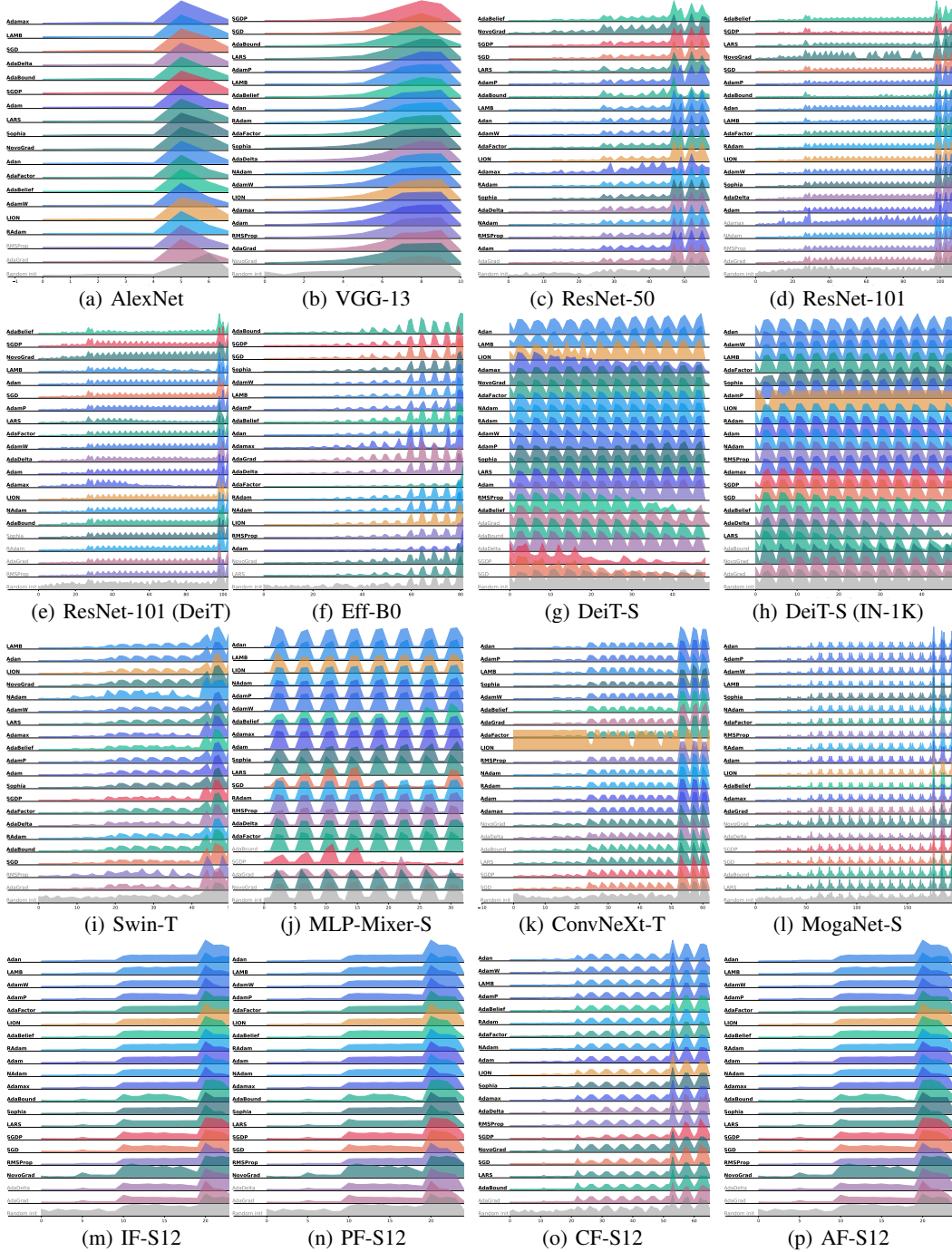


Figure A2: Ridge plot of the entropy of learned parameters on CIFAR-100. For the sub-figure of each optimizer, the X and Y axes indicate the layer indexes and the entropy of weights.

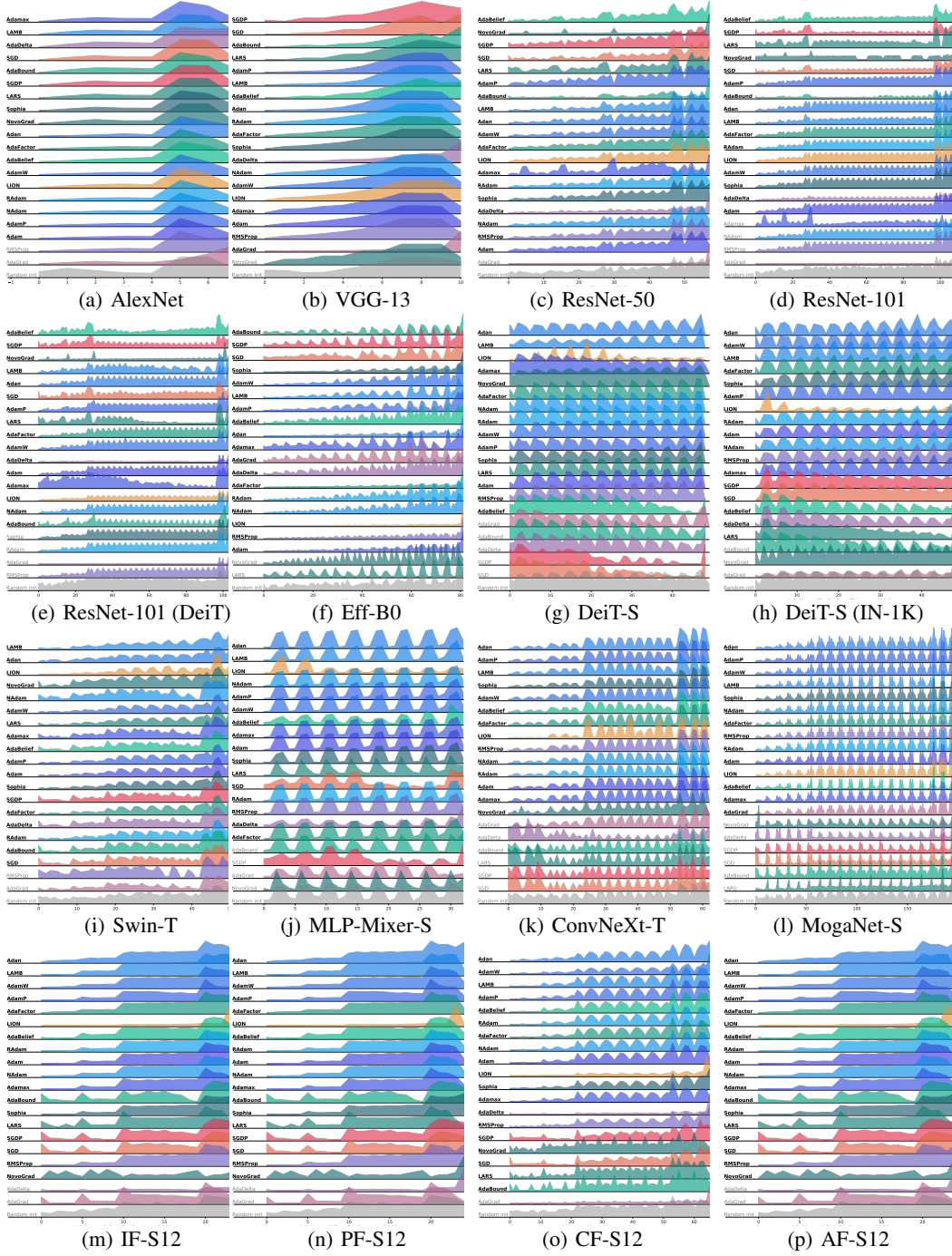


Figure A3: Ridge plot of the L_2 -norm of learned parameters on CIFAR-100. For the sub-figure of each optimizer, the X and Y axes indicate the layer indexes and the L_2 -norm of weights.

C.1 MACRO DESIGN'S INFLUENCE ON OPTIMIZATION

Our empirical inquiry commenced with a profound analysis of the macro design's impact on the optimization landscape. We executed extensive experiments utilizing a diverse array of vision backbones, ranging from Primary CNNs, which laid the groundwork for the CNN paradigm, through classical CNNs such as ResNet, which introduced a stage-wise hierarchical design, to Modern DNNs like ConvNeXt and MogaNet, which feature complex block-wise heterogeneous structures.

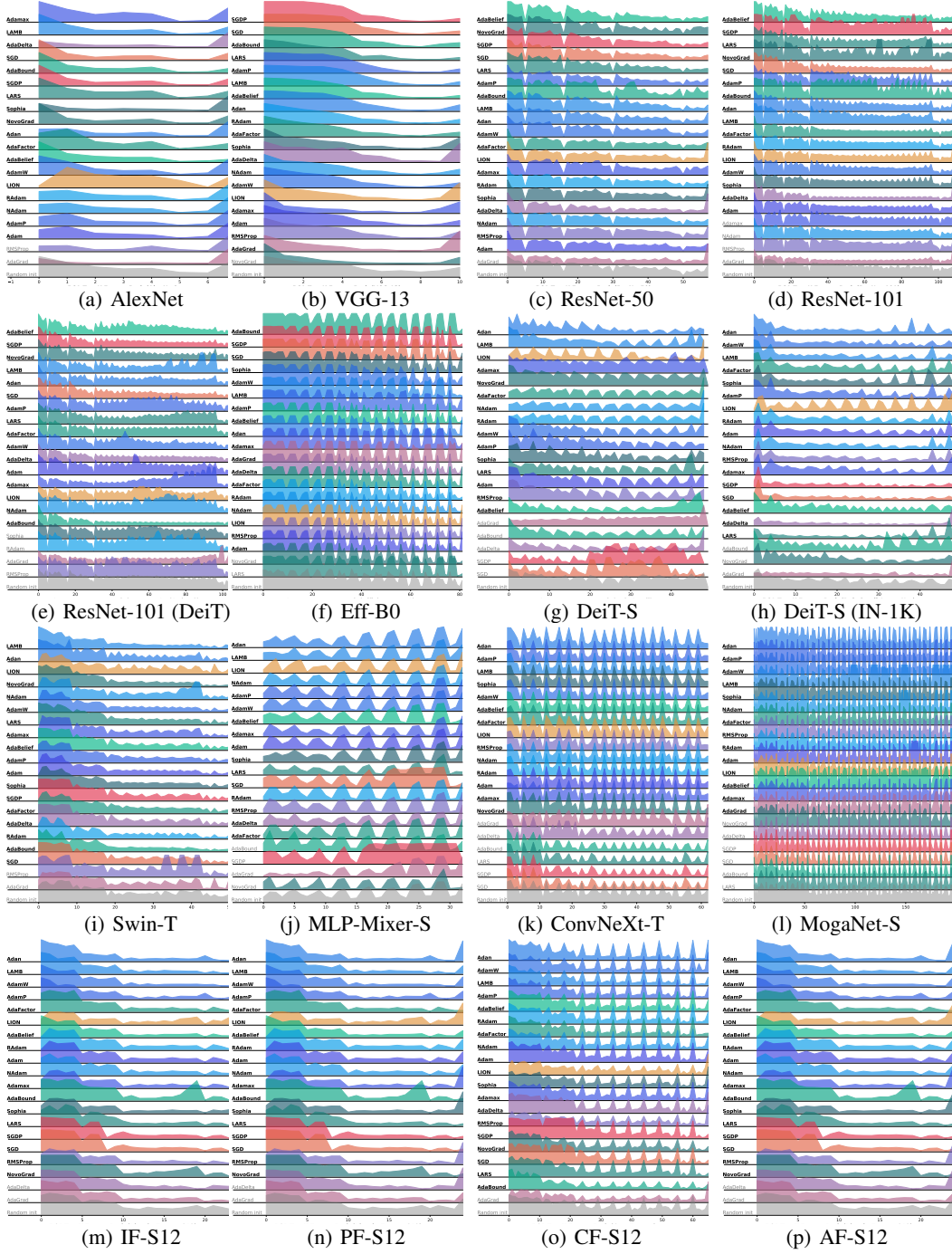


Figure A4: Ridge plot of the top-K energy PCA ratio of learned parameters on CIFAR-100. For the sub-figure of each optimizer, the X and Y axes indicate the layer indexes and the top-K PCA ratio of weights. Weights with a larger top-k PCA ratio yield skewed eigenvalue distributions, making these plots show opposite values as plots with entropy or L_2 -norm.

Our findings, as depicted in Figure 1, unveil a discernible trend: the escalation of macro design complexity corresponds with an increase in optimization complexity. This is notably evident in the juxtaposition between ResNet-50 and contemporary backbones such as MobileNetV2 and EfficientNet. While ResNet-50, with its stage-wise hierarchical architecture, exhibits a robust coupling with SGD optimizers, the latter backbones manifest a predilection for adaptive learning rate optimizers due to their intricate feature extraction mechanisms.

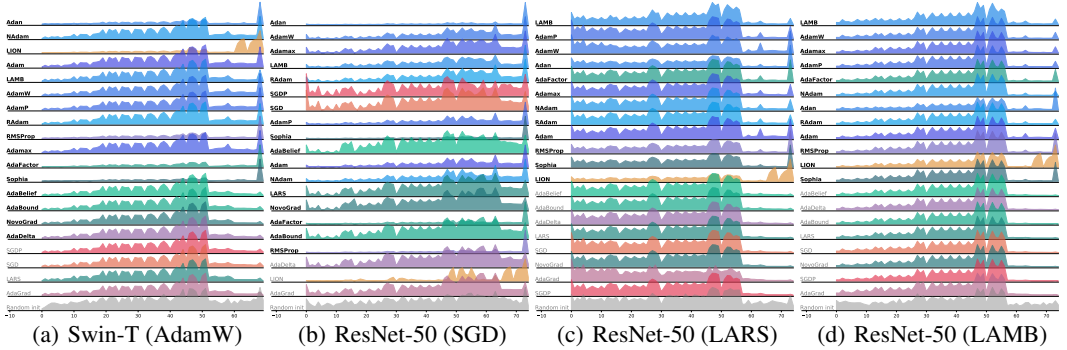


Figure A5: Ridge plot of the L_2 -norm parameter patterns for transfer learning to object detection (RetinaNet) based on Swin-T and ResNet-50 on COCO, where (a)-(d) are pre-trained by AdamW, SGD, LARS, and LAMB optimizers on ImageNet-1K. Notably, the distributions of backbone parameters are largely determined by pre-training, while the randomly initialized weights of FPN and detection head (after the 53-th or 58-th layer in Swin-T and ResNet-50) distinguish the trial patterns.

C.2 TOKEN MIXING AND OPTIMIZATION SYNERGIES

In our quest to unravel the effects of token-mixing operations on optimization, we scrutinized the performance of various token-mixing operators within the MetaFormer architecture. As meticulously detailed in Table 1, each token mixing operator—Identity, Pooling, Attention, and Convolution—presents unique challenges and sensitivities to optimizer hyperparameters.

The ConvFormer architecture, as a MetaFormer derivative, epitomizes a balanced approach to token mixing and optimization. By adopting a streamlined block-wise design and alternating between convolutional and token mixing blocks, ConvFormer mitigates BOCB and facilitates a more efficient optimization process. This approach underscores the significance of harmonizing architectural design with optimization strategies to minimize BOCB.

C.3 OPTIMIZER SELECTION AND THE BOCB NEXUS

To gauge the impact of optimizer selection on BOCB, we conducted experiments with a panoply of optimizers across diverse backbones. The results, as illustrated in Figure 5, indicate that the choice of optimizer significantly modulates the extent of BOCB. Optimizers adept at navigating complex optimization landscapes, such as those in Categories (b) and (c), exhibit robust performance across a spectrum of backbones. Conversely, Category (a) optimizers necessitate meticulous hyperparameter tuning for classical CNNs, while Category (d) optimizers manifest the most pronounced BOCB and suboptimal performance.

Our empirical analysis accentuates the critical interplay between network macro design, token mixing operations, and optimizer selection in sculpting the optimization landscape of vision backbones. The findings offer valuable insights for designing future vision backbones, emphasizing the imperative for a balanced approach that aligns backbone design with selecting appropriate optimizers.

C.4 PRE-TRAINING AND TRANSFER LEARNING

Extending our investigation to practical applications, we examined the performance of various optimizers in the context of pre-training on ImageNet-1K and subsequent transfer learning to tasks such as object detection with RetinaNet and pose estimation on COCO. As demonstrated in Table 1, optimizers like AdamW, which exhibited a reliable peak in performance during pre-training, sustained their superiority in transfer learning scenarios. This suggests that the choice of optimizer during the pre-training phase can significantly influence the transfer learning outcomes.

Our experiments also underscore the importance of a comprehensive pre-training phase that pairs vision backbones with suitable optimizers to ensure robust transfer learning capabilities. Models that underwent an extended pre-training period with optimizers like LAMB demonstrated enhanced performance compared to those with shorter pre-training durations using SGD or other optimizers.

The empirical experiments presented in this section provide a robust validation of the BOCB phenomenon and its implications for the design and optimization of vision backbones. By systematically exploring the interplay between network macro design, token mixing operations, and optimizer

selection, we have identified key factors that contribute to BOCB and provided actionable guidelines for mitigating its impact. Our findings underscore the need for a balanced approach to backbone design and optimizer selection to enhance training efficiency and performance in computer vision applications.

C.5 RULES FOR COUNTING THE OPTIMIZER RANKINGS

We have summarized and analyzed a great number of mixup benchmarking results to compare and rank all the included mixup methods in terms of *performance*, *applicability*, and the *overall* capacity. We have conducted a comprehensive meta-analysis of optimizer benchmarking results to systematically evaluate and rank a diverse array of optimization algorithms across four critical dimensions: *Performance*, *Hyperparameter Robustness*, *Backbone Optimizer Coupling Bias* (BOCB), and *Computational Efficiency*. Our methodology employs a weighted scoring system to synthesize these multifaceted evaluations:

- **Performance** (40% weight): This metric quantifies an optimizer’s efficacy across various backbone architectures, reflecting its paramount importance in algorithm selection.
- **Hyperparameter Robustness** (20% weight): Quantified as the median Manhattan distance from the optimal learning rate and weight decay configurations to the maximum average distance, this metric assesses the optimizers’ robustness to hyperparameter perturbations.
- **BOCB** (20% weight): Represented as a binary indicator (1 or 0), this factor evaluates the potential for coupling deviation between the optimizer and the backbone architecture.
- **Computational Efficiency** (20% weight): Measured by GPU memory allocation, this dimension quantifies the computational resources required by each optimizer.

The aggregation of these standardized scores yields a comprehensive ranking that serves as a robust benchmark for optimizer selection in deep learning visual backbone scenarios. This multidimensional analysis not only elucidates the relative merits of established algorithms such as AdamW—corroborating its long-standing prevalence in the community—but also highlights the potential of emerging optimizers like Adan and LAMB, particularly in contexts where BOCB or hyperparameter robustness are of paramount importance.